Herranz *et al.*
Journal of Hematology & Oncology (2025) 18:38
https://doi.org/10.1186/s13045-025-01687-1

Journal of
Hematology & Oncology

RESEARCH

Open Access

C3G promotes bone marrow adipocyte expansion and hematopoietic regeneration after myeloablation by enhancing megakaryocyte niche function

Óscar Herranz[1,2,3], Pablo Berrocal[1,2,3], Carmen Sicilia-Navarro[1,2,3], Cristina Fernández-Infante[1,2,3], Luis Hernández-Cano[1,2,3], Almudena Porras[4,5*] and Carmen Guerrero[1,2,3*]

Abstract

C3G, a Rap1 GEF, promotes megakaryopoiesis and platelet function. Using transgenic and knock-out mouse models targeting C3G in megakaryocytes, we investigated whether C3G also affects the niche function of megakaryocytes during bone marrow (BM) recovery after myeloablation induced by 5-fluorouracil (5-FU), or total body irradiation (TBI) followed by bone marrow transplantation. C3G promoted megakaryocyte maturation and platelet production during recovery, along with increased white and red blood cell counts and enhanced survival of female mice after repeated doses of 5-FU. Additionally, megakaryocytes favored adipocyte differentiation through a C3G-mediated mechanism, likely involving *Fgf1*. Changes in the number or behavior of BM megakaryocytes and adipocytes influenced the hematopoietic stem cell pool, with C3G promoting its bias towards the myeloid-megakaryocytic lineage in both 5-FU- and TBI-ablated models. Therefore, C3G could be a potential target in therapies aimed at enhancing hematopoiesis in patients undergoing chemotherapy and/or BM transplantation.

Keywords Rapgef1, Megakaryocyte, Bone marrow niche, Myeloablation, Adipocyte, Hematopoietic stem cell, Transplantation, Chemotherapy

Background

C3G (gene name *RAPGEF1*) is a Guanine nucleotide Exchange Factor (GEF) that primarily activates Rap1 GTPases [1]. It plays a pivotal role in platelet functions such as activation, aggregation [2, 3], exocytosis, spreading, and clot retraction [4, 5]. C3G also contributes to platelet-mediated angiogenesis in various pathological contexts [6]. On the other hand, the GTPase Activating Protein (GAP) Sipa1 is the main negative regulator of Rap1 GTPases in the hematopoietic system, acting as a tumor suppressor in hematological malignancies [7].

Beyond its involvement in platelet functions, C3G regulates megakaryopoiesis and thrombopoiesis under stress conditions, such as tumor cell implantation [8] and 5-fluorouracil (5-FU)-induced bone marrow (BM)

*Correspondence:
Almudena Porras
maporras@ucm.es
Carmen Guerrero
cguerrero@usal.es
[1] Centro de Investigación del Cáncer (CIC), USAL-CSIC, Campus Unamuno S/N, Salamanca, Spain
[2] Instituto de Investigación Biomédica de Salamanca (IBSAL), Salamanca, Spain
[3] Departamento de Medicina, Universidad de Salamanca, Salamanca, Spain
[4] Departamento de Bioquímica y Biología Molecular, Facultad de Farmacia, Universidad Complutense de Madrid, Ciudad Universitaria, Madrid, Spain
[5] Instituto de Investigación Sanitaria del Hospital Clínico San Carlos (IdISSC), Madrid, Spain

depletion [6]. This positive role of C3G in differentiation has also been reported for myocytes, adipocytes, neuroblasts [9] and embryonic stem cells [10]. C3G also participates in the differentiation of oval cells into hepatocytes [11]. In addition, our previous findings indicated that C3G overexpression in megakaryocytes (MKs) enhances the generation of bone marrow adipocytes (BMAs) following melanoma cell implantation [8], which supports a role for MK C3G in adipocyte expansion in response to stressors.

MKs are well-known niche regulators of hematopoietic stem cell (HSC) quiescence and activity through interactions with endothelial cells in the vascular niche [12, 13]. In resting conditions, MKs secrete factors like TGFβ1, PF4 (also known as CXCL4) and IL-6 to maintain HSC quiescence and self-renewal [12, 14]. MKs also express thrombopoietin (TPO), which further contributes to HSC quiescence [15]. In fact, ablation of MKs favors HSC proliferation [12]. However, the MK population increases following 5-FU-induced myeloablation and promotes HSC expansion by producing FGF1 [16]. MKs originate from an oligopotent megakaryocytic/erythroid progenitor (MEP) [17], but they can also arise directly from HSC or multipotent progenitor (MPP) subsets. Indeed, TPO directly promotes MK generation from biased progenitors [18].

In addition to MKs, the BM niche comprises various other cell populations including osteoblasts, osteoclasts, adipocytes, mesenchymal stem cells, and endothelial cells, among others [19]. The BM niche enhances the ability of HSCs to engraft and repopulate in transplant settings or following chemotherapy-induced myeloablation [20, 21]. To mobilize HSCs after BM depletion, disruption of the CXCR4/SDF1 axis is necessary [22], while SDF1 (also known as CXCL12) production by BM mesenchymal stromal cells is crucial for successful cell engraftment after transplantation [14, 23].

During a BM disorder or failure, such as that caused by 5-FU or irradiation, the body can initiate extramedullary hematopoiesis (EMH) to overcome the inadequate production of blood cells. As a result, organs such as the spleen take on this task, which could be reflected in splenomegaly [24].

On the other hand, it has been proposed that mature BMAs act as negative modulators of HSCs by secreting TNFα and adiponectin, thereby preserving the HSC pool [25, 26]. In fact, ablation of BMAs positively influences engraftment after BM transplantation [25]. However, BMAs contribute to hematopoietic regeneration after injury by producing SCF [26, 27], and their abundance in the BM increases following irradiation or chemotherapy, concomitantly with HSC proliferation [27, 28]. It has been described that BMAs and MKs share a reciprocal relationship. Adipocyte delipidation enhances MK maturation through the CD36 transporter present on the MK membrane, a process likely regulated by an as-yet unidentified delipidation signal from MKs [29, 30]. On the other hand, factors that regulate adipocyte differentiation, such as FGF1 [31], IGF1 [32], PREF1 [33] and IL-6 [34], are released by MKs within the BM [14, 35]. However, no direct link between these observations has been established thus far.

In this study, we investigated the role of C3G in the niche function of MKs following BM depletion induced by chemotherapy or irradiation. Our findings suggest that MK C3G positively contributes to hematopoietic recovery after myeloablation, enhancing survival. Specifically, MK C3G promotes BMA maturation and expansion both, in vitro and in vivo, through the release of factors from MKs that facilitate, directly or indirectly, adipocyte differentiation. Additionally, MK C3G supports the myeloid branch of hematopoiesis during recovery, particularly influencing the megakaryocytic and erythroid lineages.

Methods

Mouse models

The MK-specific transgenic (tgC3G^{Pf4}) and conditional knock-out (*Rapgef1*$^{fl/fl}$;*Pf4*-Cre$^{+/-}$, hereinafter C3G^{Pf4}-KO) mouse models for C3G used in this work have been described and characterized previously [2–6, 8]. wtC3G^{Pf4} and *Rapgef1*$^{fl/fl}$;*Pf4*-Cre$^{-/-}$ (hereinafter C3G^{Pf4}-wt) are their respective control mice. C57BL/6 *Ly5.1*-expressing mice (Ly5.1$^{+/+}$) were purchased from Charles River Laboratories (France) for transplant experiments. The Sipa1-KO mouse model was described in [7, 36]. All mice used were 6- to 10-week-old.

5-FU-induced myeloablation

5-FU was freshly prepared in 0.9% NaCl with 10% DMSO at 37 °C with vigorous shaking. Mice were injected intraperitoneally (i.p.) with a sublethal dose of 150 mg/kg 5-FU (Merck Millipore, #F6627) to induce myelosuppression. Their recovery was then assessed for 21 days.

To test the effect of C3G on sensitivity to noxious injury, mice were injected weekly with 150 mg/kg 5-FU and monitored for survival. According to ethical guidelines, mice were euthanized when they showed a 20% body-weight reduction or two or more moderate grimaces of pain [37].

Bone marrow extracts

BM from the femur and tibia was collected by centrifugation method [38, 39]. Briefly, a femur and tibia were cut open and placed in nested tubes. BM was collected by spinning out the bones onto 100 µL of PBS containing

10% FBS. A homogeneous cellular suspension was prepared by adding 900 µL of PBS with 10% FBS and gently pipetting up and down. This BM extract was used for further applications.

For experiments involving Sipa1-KO and wtSipa1 mice, BM extracts were obtained by crushing the femur and tibia with a mortar and pestle in PBS with 10% FBS and filtering the resulting cell solution through a 70-µm filter.

Evaluation of BM cellularity

Twenty microliters of a 1/10 dilution of the BM extracts (from one femur and one tibia) were mixed with 380 µL of Muse® Count & Viability reagent (Merck Millipore, #MCH100102). This solution was then analyzed in a Muse® Cell Analyzer (Merck Millipore) using the appropriate software module.

Analysis of hematological parameters

Whole blood was collected via submandibular vein puncture in EDTA-coated tubes (Sarstedt, #41.1395.005) and analyzed using an ADVIA 120 Hematology System (Siemens AG).

Determination of platelet number by flow cytometry

In addition to hemocytometry analysis, platelet counts were also determined using a BD Accuri™ C6+ cytometer, as previously described [3].

Immunophenotyping of HSPCs

Hematopoietic stem and progenitor cell (HSPC) populations were identified according to the scheme by [40]. Briefly, erythrocytes from BM extracts were lysed in ACK buffer (0.155 M NH_4Cl, 10 mM $KHCO_3$, 10 mM EDTA pH 7.4) for 5 min at 4 °C. After washing and resuspension in the same buffer, cells were stained with the following antibodies: FITC-Lin (#133302, 1/100), PE-c-Kit (#105,808, 1/333), APC-Sca-1 (#108112, 1/100), PE/Cy7-CD16/32 (#101318, 1/133), PerCP/Cy5.5-CD34 (#128608, 1/50), BV510-CD127 (#135033, 1/80), all from BioLegend, as well as PE/CF594-CD135 (#562537, 1/50), from BD Biosciences. One million cells were acquired in a BD FACSAria III flow cytometer.

In experiments involving BM isolated from transplanted mice, the PE/Cy7-CD16/32 antibody was replaced by PE/Cy7-CD45.2 (#109830, 1/100) antibody, and Pacific Blue™-CD45.1 (#110722, 1/100) (both from BioLegend) was added to the cocktail to distinguish donor and host cells.

Immunophenotyping of mesenchymal stem cells and adipocyte-committed progenitors

BM $CD45^{-}CD31^{-}Sca\text{-}1^{+}$ cells were identified as mesenchymal stem cells (MSCs) if they were positive for the CD24 marker; or as adipocyte-committed progenitors (APCs), if they were negative for CD24, according to [28]. BM cells were erythrocyte-lysed, washed, and resuspended in PBS with 3% FBS. Cells were stained with FITC-CD31 (#102405, 1/100), FITC-CD45 (#103,107, 1/100), PE-CD24 (#101807, /100) and APC-Sca-1 (#108112, 1/75) from BioLegend, for 30 min on ice in the dark. Samples were acquired using a BD Accuri™ C6+ cytometer. At least 5×10^5 events were recorded.

Immunophenotyping of mature lineages

Whole blood was collected via submandibular vein puncture in EDTA-coated tubes (Sarstedt, #41.1395.005). After lysing erythrocytes, cells were resuspended in 50 µL of PBS with 3% FBS and stained with the following antibody combinations (from BioLegend): PE-CD11b (Mac-1, #101207, 1/100) and APC-Ly-6G/Ly-6C (Gr-1, #108412, 1/100) for the identification of neutrophils, FITC-CD4 (#100509, 1/100), PE-CD8a (#100707, 1/100) and APC-CD3 (#100236, 1/100) for detecting T lymphocytes, and FITC-B220 (#103205, 1/100) for detecting B lymphocytes.

In experiments involving the analysis of peripheral blood (PB) from transplanted mice, PerCP/Cy5.5-CD45.1 (#110728, 1/100) and APC-CD45.2 (#109814, 1/100) antibodies from BioLegend were added to the cocktails to distinguish donor and host cells. In this setting, FITC-Ly-6G/Ly-6C (Gr-1, #108405, 1/100) antibody was used instead of APC-Ly-6G/Ly-6C, and the APC-CD3 antibody was omitted.

In all cases (except for transplant settings), cells were resuspended in PBS containing 3% FBS and 1 µg/mL propidium iodide (PI) before analysis to exclude dead cells. Samples were acquired using a BD Accuri™ C6+ cytometer. At least 1.5×10^4 events were recorded. All cytometry data were analyzed using FlowJo v10.7.1 software.

Bromodeoxyuridine (BrdU) incorporation

BrdU (MedChemExpress, #HY-15910) was prepared in PBS at a final concentration of 10 mg/mL. Mice were i.p. injected with a single dose of 100 mg/kg. Sixteen hours later, the mice were sacrificed, and bone marrow harvested. After lysing erythrocytes, cells were stained with lineage markers FITC-Lin (BioLegend, #133302, 1/100) for 20 min on ice in the dark and fixed with 4% paraformaldehyde (PFA, Sigma-Aldrich, #P6148) in PBS for 20 min at RT. Cells were then permeabilized by adding 300 µL of 0.5% Triton-X100 (Sigma-Aldrich, #X100) in PBS for 15 min at RT and treated with 30 µg of DNase I (Roche, #10104159001) in 100 µL PBS for 1 h at 37 °C. After washing, the cell pellet was resuspended in 50 µL PBS with 1% FBS and stained with PE/Cy7-BrdU antibody (BioLegend, #364117, 1/100) for 20 min at RT in the

dark. Cells were analyzed using a BD FACSAria III flow cytometer, and data were analyzed with FlowJo v10.7.1 software.

Maturity of MKs

BM cells were stained with PE-CD61 (eBiosciences, #12–0611-81, 1/100), a MK marker, and APC-CD42 (BioLegend, #148505, 1/100), a marker of mature MKs [41]. At least 2×10^4 double positive events were acquired using a BD Accuri™ C6+ cytometer. Analysis was carried out using FlowJo v10.7.1 software.

Hematoxylin–eosin (H&E) staining for MK and BMA counting

Femora were harvested and fixed in 4% formaldehyde for 24 h at 4 °C, following decalcification in Osteosoft (Sigma-Aldrich, #1.01728). Femora were paraffin-embedded, and sectioning was performed using a HistoCore Autocut microtome (Leica). Tissue sections were stained with H&E (Casa Álvarez, Spain, #10–3002) at the CIC Pathology Unit. Images were acquired with an Olympus BX51TF microscope coupled to an Olympus DP74 camera.

MKs were manually counted, as they are easily recognized as large pinkish cells with multilobulated dark purple nuclei. A semi-automatic approach was used for BMAs, which can be identified as large, rounded empty-appearing spaces with a thin bright cytoplasmic boundary in pink and peripheral nuclei. First, images were converted to 8 bits and a threshold was automatically established using "Triangle" algorithm. Second, *open*, *close*, and *fill holes* binary operations were applied. Finally, object recognition was checked, and BMAs not considered by the algorithm were manually identified. The numbers of MKs and BMAs were quantified relative to the bone marrow area.

Lineage-negative enrichment of BM via MACS

BM cell extracts from tgC3G^{Pf4}, C3G^{Pf4}-KO mice and their wild-type littermates were enriched for progenitors using magnetic-activated cell sorting (MACS). Briefly, BM cells were resuspended at a concentration of 200×10^6 cells/mL in PBS with 10% FBS and the following purified antibodies from BioLegend added: anti-Gr-1 (#108401, 1/400), anti-CD11b (#101201, 1/400), anti-CD19 (#115501, 1/200), anti-CD3 (#100201, 1/200), anti-Ter119 (#116201, 1/200). Following incubation, washed Sheep anti-Rat IgG Dynabeads™ (Thermo Fisher Scientific #11035) were added, following manufacturer's instructions, to capture mature cells. The cell suspension was then separated using the DynaMag™-2 magnet (Thermo Fisher Scientific, #12321D). Supernatants containing progenitor-enriched BM cells were recovered, centrifuged, and resuspended at 2×10^6 cells/mL in DMEM with 20% FBS and 50 ng/mL TPO. Finally, 1×10^6 cells were seeded in the upper chamber of a 0.4 µm cell culture insert to initiate the co-culture with 3T3-L1 cells (see next).

Adipokine evaluation of BM supernatants

Seven days after 5-FU administration, BM supernatants from at least three mice per genotype were pooled and 300 µL of sample was assayed using the Proteome Profiler Mouse Adipokine Kit (R&D Systems, #ARY013) according to manufacturer's instructions. Blots were developed on Super RX-N X-ray films (Fujifilm) and scanned using an Epson V700-Photo scanner. Densitometric analysis was carried out using ImageJ/FiJi analysis software.

Co-culture of MKs and 3T3-L1 pre-adipocytes

To study the contribution of MKs to adipocyte differentiation and/or expansion, we established an indirect co-culture system based on [29]. Briefly, 1×10^5 3T3-L1 cells were seeded in 400 µL of maintenance medium (MM: DMEM + 10% calf serum (CS) + 1% penicillin/streptomycin) in a 24-well plate coated with 5 µg/cm^2 collagen type I (Corning, #354,236). After 24 h, MM was replaced with differentiation medium I (DM-I: MM containing 500 µM isobutylmethylxanthine (IBMX), 1 µM dexamethasone (DEX), 5 µM troglitazone (TROG) and 10 µg/mL insulin), for two days to initiate commitment. Subsequently, cells were cultured in differentiation medium II (DM-II: MM + 10 µg/mL insulin) until day 4. From day 4, two conditions were tested: (i) cells were maintained in DM-II or (ii) in MM (i.e., without insulin), with half of the culture medium replaced every 2 days until day 8.

To evaluate the potential contribution of MKs to this process, either wtC3G^{Pf4}/tgC3G^{Pf4} or C3G^{Pf4}-wt/C3G^{Pf4}-KO lineage-negative (Lin$^-$) cells (1 x 10^6) isolated via MACS were seeded on day 4 in the upper chamber of a 0.4 µm Boyden chamber/Transwell insert (Costar®, #3470) in DMEM with 20% FBS and 50 ng/mL TPO to promote the differentiation of progenitor cells towards MKs. One Transwell insert without progenitor cells was used to account for effects derived from TPO addition. On days 6 and 8, BODIPY™ staining was performed to evaluate lipid content in differentiated 3T3-L1 cells using image analysis. Afterward, cells were lysed in NZYol reagent (NZYTech # MB18501) for RNA isolation.

For inhibition assays, TPO-stimulated Lin$^-$ cells were treated with 70 µM suramin (MedChemExpress, HY-B0879A) to unselectively block growth factors secreted by HSPCs/MKs. Alternatively, 3T3-L1 cells were treated with 0.5 µM infigratinib (NVP-BGJ398), a selective FGFR1-3 inhibitor [42].

BODIPY™ staining of lipid droplets

On days 6 and 8, culture medium was removed, and 1 µg/mL BODIPY™ 493/503-containing DMEM without phenol red (Gibco™, #21041025) was added to the wells and cells were incubated for 20 min. After staining, the BODIPY™-containing medium was discarded and fresh DMEM without phenol red was added for image acquisition in an Incucyte® SX5 Instrument (Sartorius). Thirty-six pictures per well were captured using the AI Scan module and a 20X objective. Raw phase and raw green images were exported and analyzed using CellProfiler v4.2.6 software. The configuration used was based on the method described in [43] with some modifications: (i) the diameter of objects was set at 1–80 px, (ii) a threshold correction factor of 1.2 was applied, and (iii) the method to identify individual objects within clumped objects was changed to "Propagate". For images taken on day 8, a threshold correction factor of 1.6 was used instead.

BM transplantation

BM cells from at least three mice were pooled and counted using a Beckman Coulter Z2 hemocytometer. The cell concentration was adjusted to 2×10^6 cells/200 µL in sterile PBS. The cell solution was kept on ice until injection.

Female tgC3G^{Pf4}, C3G^{Pf4}-KO mice and their corresponding wild-type littermates were irradiated with two doses of 5.5 Gy separated by 4 h. After 2–3-h recovery period, 2×10^6 pooled whole BM cells from Ly5.1/CD45.1 donors were injected via the lateral tail vein. The number of neutrophils, T lymphocytes, and B lymphocytes in PB was assessed monthly until the 9th month, when mice were sacrificed to evaluate potential changes in BM and spleen.

RT-qPCR analysis

cDNA was synthesized from MK and 3T3-L1 cell RNA using the NZY First-Strand cDNA Synthesis kit (NZYTech, #MB12501). MKs were freshly isolated from steady-state BM by FACS as CD41/CD42 double positive cells and immediately added to the lysis buffer. Gene expression was assessed by qPCR using SYBR Green master mix (NZYTech, #MB22202) and primers listed in Additional file 1, Suppl Table 1. Primers were designed using the Primer-BLAST Tool. In the analysis of the expression of genes in Sipa1-KO MKs, TaqMan probes were used (Suppl Table 2). Data were analyzed using the $2^{(-\Delta\Delta Ct)}$ method [44]. β-actin (*Actb*) or hypoxanthine guanine phosphoribosyl transferase (*Hprt*) genes were used as housekeeping genes, as indicated.

Statistical analysis

Unless otherwise specified, all the results were reported as mean ± standard error of the mean (SEM) from at least three independent experiments, each including multiple replicates. Statistical analyses were performed using GraphPad Prism v8.2.1. Data normality was assessed with Shapiro–Wilk tests. For comparisons between two experimental groups, a *t*-test was used. To evaluate differences among three or more groups, one-way or two-way ANOVA was applied, depending on whether one or two factors were analyzed. ANOVA tests were followed by Fisher's Least Significant Difference (LSD) post-hoc test. The choice of statistical test was based on the normality and homoskedasticity of the data. For Kaplan–Meier survival analysis, a log-rank test was performed. *p* values less than or equal to 0.05 were considered statistically significant.

Results

C3G boosts MK maturation following myeloablation, leading to hematopoiesis recovery

Previous data from our group have confirmed that C3G promotes megakaryocytic differentiation both in vitro and ex vivo in response to TPO stimulation [8]. Additionally, injection of TPO or 5-FU in MK-specific C3G-overexpressing mouse models increases platelet count, whereas C3G ablation results in a decrease in platelet levels [6, 8].

To further investigate the role of C3G in MK physiology under biological stress conditions, we induced myelosuppression in tgC3G^{Pf4} and C3G^{Pf4}-KO mice, along with their respective wild-type siblings through i.p. administration of a sublethal dose of 5-FU. Recovery was monitored at several time points (Fig. 1A). As previously reported using flow cytometry [6], hemocytometric analysis revealed a significant increase in platelet rebound in tgC3G^{Pf4} mice (Fig. 1B), while deletion of C3G delayed platelet count recovery (Fig. 1C). Similarly, white blood cell (WBC) counts recovered faster in tgC3G^{Pf4} mice, surpassing resting levels (Fig. 1D), accompanied by elevated red blood cell (RBC) and hemoglobin levels (Fig. 1E, F). In contrast, WBC counts remained lower in C3G^{Pf4}-KO mice, compared to C3G^{Pf4}-wt mice, during recovery (Fig. 1G), with no effect on RBC counts or hemoglobin levels (Fig. 1H, I). This suggests that C3G overexpression in MKs may help mitigate the decline in blood cell populations, other than platelets, following chemotherapy.

Comparative analysis of hematoxylin–eosin-stained femur sections revealed that the number of MKs in the BM of tgC3G^{Pf4} mice 7 days after 5-FU administration was significantly lower than in wtC3G^{Pf4} mice, though the numbers equalized at later recovery stages (Fig. 1J,

K). Conversely, C3G^{Pf4}-KO mice showed a significant increase in MK numbers in the BM compared to wild-type controls (Fig. 1L, M), with differences becoming significant 10 days post-treatment. To determine whether MK maturity correlated with platelet production, we examined the surface levels of CD42 and CD61 in BM extracts using flow cytometry. As expected, MKs from tgC3G^{Pf4} mice were more mature than those from C3G^{Pf4}-KO mice, compared with their respective control littermates (Fig. 1N, O). This difference in maturity was also evident in the bone marrow sections, where MKs in tgC3G^{Pf4} femora were notably larger than those in wtC3G^{Pf4} marrow (Fig. 1P), with no differences between C3G^{Pf4}-KO and C3G^{Pf4}-wt mice (Fig. 1Q). This suggests that C3G may regulate MK differentiation, maturation and platelet production upon 5-FU treatment, with this process being delayed in the absence of C3G. Consistent with other reports [26, 45], the distribution of MKs along the femoral marrow was not random, with a progressive enrichment from the proximal to the distal region, and the most notable differences between genotypes occurring in the latter region (Fig. 1R, S).

Bone marrow adipocytes (BMA) expand parallel to C3G expression in MKs after 5-FU

We previously described a significant increase in BMA density following melanoma cell implantation in tgC3G^{Pf4} mice [8], suggesting that C3G expression in MKs might influence the response of BM stromal cells to an insult. Based on this, we first explored whether MK C3G affects the adipocyte progenitor cell (APC) population during recovery from 5-FU treatment. Seven days after treatment initiation, APCs were significantly less abundant in the BM of tgC3G^{Pf4} mice (Fig. 2A), whereas C3G^{Pf4}-KO mice exhibited the opposite trend (Fig. 2B). These changes in the progenitor population resulted in a higher number of BMAs in the femora of tgC3G^{Pf4} mice (1.6-fold increase) by day 10 compared to their wtC3G^{Pf4} littermates, likely due to a role of MK C3G in the differentiation of APCs into BMAs (Fig. 2C, D and Suppl Fig. 1A). Supporting this, the number of BMAs in the BM of C3G^{Pf4}-KO mice was lower than that in C3G^{Pf4}-wt mice (Fig. 2E, F and Suppl Fig. 1B). This suggests a defective differentiation capability of APCs upon C3G deletion in MKs, resulting in the observed accumulation of adipocyte progenitors (Fig. 2B). Furthermore, BMAs from tgC3G^{Pf4} mice were on average 57.64 ± 14.95 μm^2 larger than those from wtC3G^{Pf4} mice (Fig. 2C, G). In contrast, no differences in adipocyte size were detected in the C3G^{Pf4}-KO genotype (Fig. 2E, H), indicating that the observed variations in total marrow adipose tissue (MAT) were due to MK C3G-induced MAT hyperplasia rather than hypertrophy. No differences were observed in either the number of adipocytes or their size before and after recovery (21 days) from 5-FU treatment (Fig. 2C, E, and Suppl Fig. 1C–F).

These changes in adipogenesis observed during mid-recovery from 5-FU suggest that factors within the BM microenvironment of both tgC3G^{Pf4} and C3G^{Pf4}-KO mice differ from those of their corresponding wild-type counterparts. To address this, we evaluated adipokine levels of pooled BM supernatant samples using a specific Proteome Profiler array. The results shown in Fig. 2I and Suppl Fig. 2 indicate a differential release of factors between tgC3G^{Pf4} and C3G^{Pf4}-KO BM, compared to their respective controls. It is worth noting the lower levels of IL-6 in tgC3G^{Pf4} BM, which plays a negative role in adipogenesis by downregulating PPARγ and C/EBPα transcription factors [46]. In contrast, IL-6 levels were higher in C3G^{Pf4}-KO BM compared to C3G^{Pf4}-wt. The same pattern was found for RAGE and RANTES (CCL5), both playing a role in inflammation and insulin resistance associated with obesity [47, 48]. Although only IL-6 has been described to be secreted by MKs [49], these results support the observed increase in BMA in tgC3G^{Pf4}

(See figure on next page.)

Fig. 1 MK C3G promotes hematopoietic recovery following 5-FU treatment by enhancing megakaryocyte (MK) maturation (**A**) Scheme of 5-FU-induced myeloablation. Blood drops indicate the days of blood extraction. Femurs indicate the days of femur and BM harvest. Platelet count in (**B**) tgC3G^{Pf4} and (**C**) C3G^{Pf4}-KO mice and their controls. Evaluation of (**D**, **G**) WBC, (**E**, **H**) RBC, and (**F**, **I**) hemoglobin in (**D**–**F**) tgC3G^{Pf4} and (**G**–**I**) C3G^{Pf4}-KO and their controls. Data (mean ± SEM) correspond to two independent experiments. wtC3G^{Pf4}, n = 4; tgC3G^{Pf4}, n = 5; C3G^{Pf4}-wt, n = 5; C3G^{Pf4}-KO, n = 5. (**J**, **L**) Graphics showing the mean ± SEM of MK count in the first 5 mm of femoral BM from the growth plate, at the indicated days after 5-FU, in (**J**) wtC3G^{Pf4} and tgC3G^{Pf4} and in (**L**) C3G^{Pf4}-wt and C3G^{Pf4}-KO. (**K**, **M**) Representative photomicrographs of BM sections stained with H&E. Arrowheads indicate MKs. The insets show a 2.5X magnification of the regions highlighted in the images. Scale bar: 0.25 mm. (**N**, **O**) Normalized counts (mean ± SEM) of mature MKs (CD42$^+$CD61$^+$ cells) by flow cytometry in BM extracts from (**N**) tgC3G^{Pf4}, and (**O**) C3G^{Pf4}-KO mice and their controls at the indicated days after 5-FU. (**P**, **Q**) Violin plots show the median size of MKs in the inner part of the diaphysis. (**R**, **S**) MK (mean ± SEM) quantification along (**R**) wtC3G^{Pf4} and tgC3G^{Pf4} femora 7 days after 5-FU injection, and (**S**) C3G^{Pf4}-wt and C3G^{Pf4}-KO femora 10 days after 5-FU injection. Two to three independent experiments were performed per day of analysis. wtC3G^{Pf4}, n = 4–6; tgC3G^{Pf4}, n = 4–8; C3G^{Pf4}-wt, n = 4–6; C3G^{Pf4}-KO, n = 4–6. *p*-values in (**B**–**I**, **J**, **L**, **R**, **S**) were calculated using two-way ANOVA with uncorrected Fisher's LSD post-hoc test. Unpaired *t*-test was used in (**N**–**Q**). *$p \le 0.05$. **$p \le 0.01$. ***$p \le 0.001$

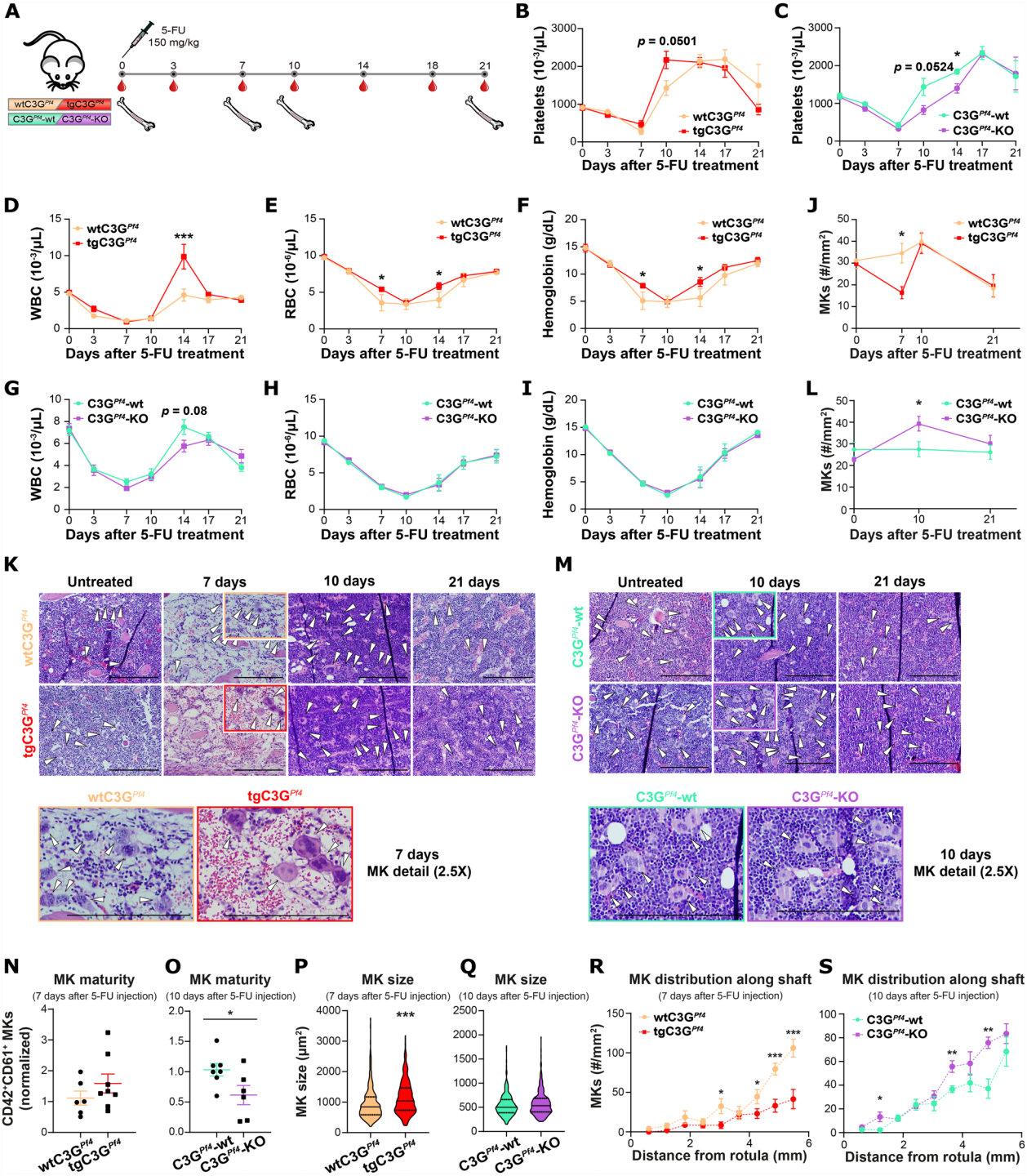

Fig. 1 (See legend on previous page.)

BM, and suggest that C3G may promote the differential release of MK factors that favor adipogenesis.

C3G from MKs promotes the differentiation of 3T3-L1 pre-adipocytes

The aforementioned results suggest that MKs may influence BMA differentiation. Previous studies have shown that MKs promote the delipidation of adipocytes, which,

in turn, enhance MK differentiation and maturation [29]. However, to our knowledge this is the first report suggesting a potential role for MKs in BMA differentiation.

To determine whether the changes observed in the BMA population in vivo were driven by signals from MKs that directly affect adipocytes, and whose release is modulated by C3G, we established an in vitro assay. This consisted of the indirect co-culture of committed pre-adipocyte 3T3-L1 cells with MKs, using a Transwell system. Freshly MACS-isolated Lin^- progenitor cells, cultured in the presence of TPO to induce megakaryocytic differentiation, were seeded in the upper chamber of the Transwell containing in the lower chamber a 4-day culture of pre-differentiated 3T3-L1 cells (Fig. 2J). This setup was maintained for an additional 4 days, and adipocyte differentiation was assessed on days 6 and 8. Notably, no differences were found between 3T3-L1 cells grown alone (control condition) or in the presence of TPO in the upper chamber of the Transwell system, ruling out any potential effect of TPO (data not shown), consistent with findings by Valet et al. [29]. However, contrary to Valet´s findings, our results suggest that the indirect co-culture of 3T3-L1 cells with HSPCs/MKs enhanced lipid synthesis in the 3T3-L1 cells, particularly during the first 2 days (Fig. 2K, L and Suppl Fig. 3A, B), regardless of the absence (Fig. 2K, L) or presence (Suppl Fig. 3A, B) of insulin in the culture medium. Notably, Lin^- progenitor cells in the upper chamber differentiated similarly across all four genotypes analyzed throughout the assay (data not shown). In cultures without insulin (MM medium), adipocyte differentiation increased in all conditions, as evidenced by a higher number of lipid droplets (Fig. 2M) and an increase in their size (Fig. 2N). Furthermore, 3T3-L1 cells co-cultured with HSPCs/MKs from tgC3G^{Pf4} mice exhibited higher lipid droplet content compared to those co-cultured with wtC3G^{Pf4} cells (Fig. 2M). This effect was also observed under DM-II conditions (Suppl Fig. 3C), closely reflecting the in vivo results (Fig. 2C, D, G).

Conversely, in 3T3-L1 cultures without insulin, a trend toward reduced lipid droplet size was observed when C3G^{Pf4}-KO HSPCs/MKs were in the upper chamber of the Transwell system (Fig. 2N). Interestingly, when insulin was present, C3G deficiency in HSPCs/MKs promoted lipid droplet formation in 3T3-L1 cells (Suppl Fig. 3C), though these droplets were significantly smaller than those in 3T3-L1 cells maintained with factors from C3G^{Pf4}-wt HSPCs/MKs (Suppl Fig. 3D).

Differentiation of 3T3-L1 cells under the influence of HSPCs/MKs was further enhanced after 4 days of co-culture (day 8 of differentiation), even in the absence of insulin, regardless of genotype (Suppl Fig. 3E–H). This mirrored the effects seen after 2 days of co-culture (day 6 of differentiation) in the presence of insulin (Suppl Fig. 3A–D).

Interestingly, all cells cultured under cues from HSPCs/MKs exhibited fewer lipid droplets compared to control cells (Suppl Fig. 3G), likely due to fusion into larger droplets, as suggested by the increase in droplet size across all conditions (Suppl Fig. 3H). Thus, the variations in BMA area observed in femur sections (Fig. 2G, H) were recapitulated in this in vitro system. Unfortunately, quantitative analysis of 4-day co-cultures with insulin was not feasible due to cell overgrowth and detachment. However, qualitative observations suggested increased proliferation of 3T3-L1 cells influenced by factors secreted by tgC3G^{Pf4} HSPC/MKs. Notably, although factors from C3G^{Pf4}-KO TPO-stimulated progenitors promoted greater lipid accumulation in 3T3-L1 cells in the absence of insulin after 4 days of co-culture (day 8) (Suppl Fig. 3F), these co-cultures displayed slower growth (and

(See figure on next page.)

Fig. 2 MK C3G promotes BMA expansion following 5-FU-induced BM depletion (**A**, **B**) Mean ± SEM of APC ($CD45^-CD31^-Sca\text{-}1^+CD24^-$) percentage within the MSC compartment in BM from (**A**) tgC3G^{Pf4} and (**B**) C3G^{Pf4}-KO mice and their controls. (**C**, **E**) H&E-stained BM sections of femurs at the indicated days post-5-FU treatment. The insets show a three-fold magnification from the 10-day images. Scale bar: 0.25 mm. (**D**, **F**) BMA number/total marrow area normalized to controls. (**G**, **H**) Violin plots depict the median area of the counted adipocytes. Three to five independent experiments were performed per day of analysis. Statistics were calculated using two-way ANOVA with uncorrected Fisher's LSD post-hoc test (**A**, **B**) and unpaired *t*-test (**D**, **F**, **G**, **H**). wtC3G^{Pf4}, n = 4–7; tgC3G^{Pf4}, n = 3–8; C3G^{Pf4}-wt, n = 6–11; C3G^{Pf4}-KO, n = 5–11. (**I**) Adipokine content in BM supernatants from either tgC3G^{Pf4} or C3G^{Pf4}-KO mice compared to their controls 7 days after 5-FU administration. Quantification was performed in short or long exposures of the Proteome Profiler membranes as indicated in Suppl Fig. 2. (**J**) In vitro setting for the analysis of MK influence on adipocyte differentiation. (**K**, **S**) Representative images of 3T3-L1 cells co-cultured without (3T3-L1) or with HSPCs/MKs of the indicated genotypes (**K**) in the absence of insulin and (**S**) under the effect of inhibitors. Scale bar: 0.2 mm. Violin plots showing (**L**, **T**) BODIPY™ mean fluorescence intensity, **(M**, **U)** number and (**N**) mean size of each lipid droplet. In each assay, 24 to 36 fields were analyzed per condition. Three independent experiments were performed in (**K**–**N**). Statistical analysis was performed using one-way ANOVA with uncorrected Fisher's LSD post-hoc test. Unless directly stated on the graph, significance was indicated as follows: * *vs* Ctrl sample; # *vs* the corresponding wild-type. One symbol $p \le 0.05$, two symbols $p \le 0.01$, three symbols $p \le 0.001$. a.u.: arbitrary units; px: pixels. *ns*: non-significant. (**O**–**R**) Mean ± SEM of the $\log_2$(Fold change) of mRNA expression of (**O**) *Fgf1*, (**P**) *Igf1*, (**Q**) *Pref1*, and (**R**) *Il6* in $CD41^+CD42^+$ MKs from the BM of tgC3G^{Pf4}, C3G^{Pf4}-KO mice and their wild-types. *$p \le 0.05$

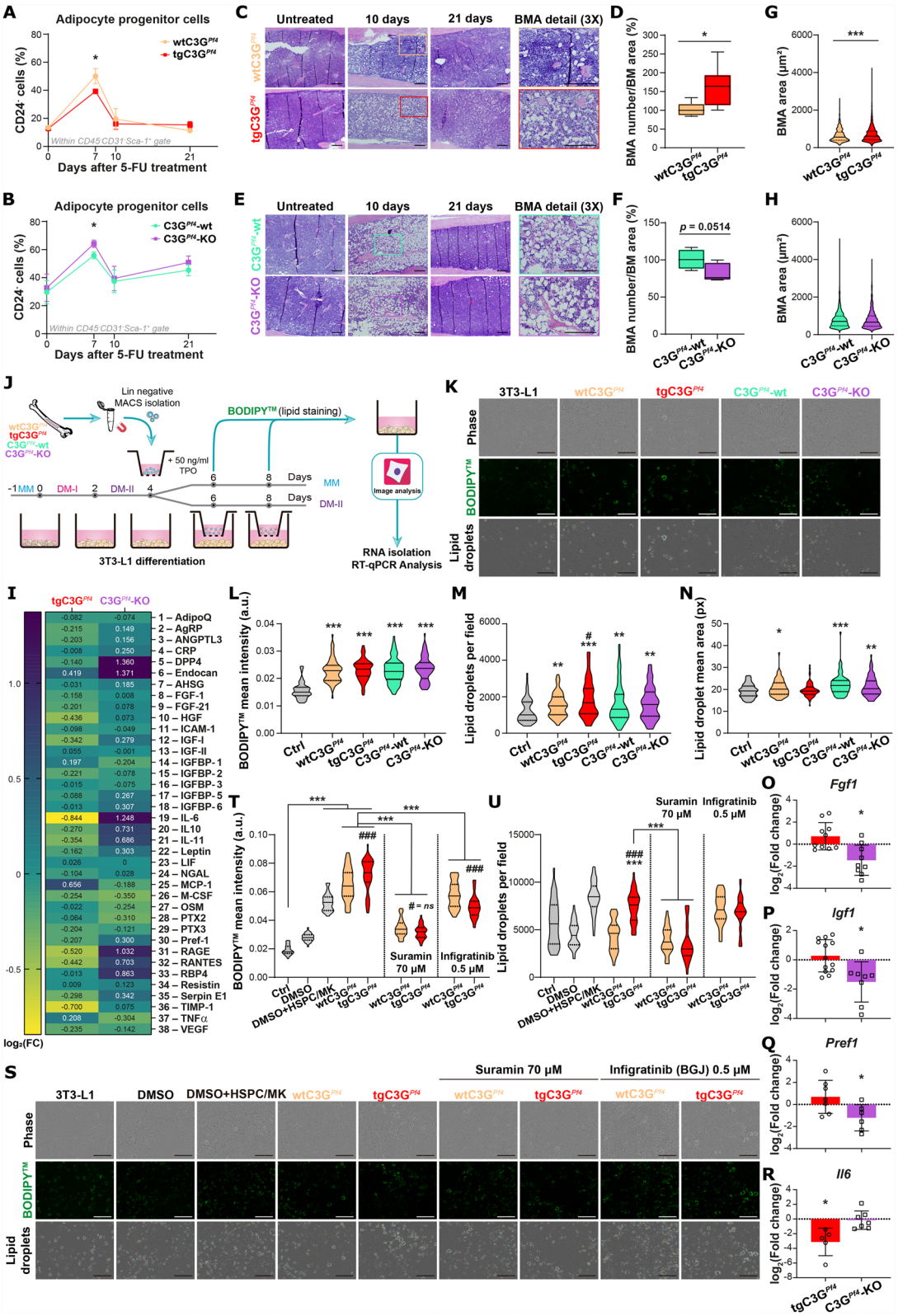

Fig. 2 (See legend on previous page.)

less cell detachment) in DM-II medium, compared to cells influenced by factors from C3G^{Pf4}-wt HSPC/MKs (Suppl Fig. 3I).

C3G modulates the expression of MK genes involved in BMA differentiation, eventually enhancing the expression of adipocyte differentiation genes in 3T3-L1 cells

Since our results suggested that factors secreted by MKs could modulate adipocyte differentiation, we next explored the expression of candidate genes, such as *Fgf1*, *Igf1*, *Pref1* and *Il6* in freshly isolated CD41^{+}/CD42^{+} MKs from the different genotypes. The expression of all these genes, with the exception of *Il6,* was reduced in MKs lacking C3G (Fig. 2O–R), potentially explaining the smaller lipid droplets observed when C3G^{Pf4}-KO HSPCs/MKs were present in the environment (Fig. 2N and Suppl Fig. 3D, H). Although not statistically significant, there was a general trend toward increased expression of *Fgf1*, *Igf1 and Pref1* in tgC3G^{Pf4} MKs compared to wtC3G^{Pf4} MKs (Fig. 2O–Q). In addition, a significant positive correlation was found between the expression of C3G (*Rapgef1*) and *Fgf1* (Suppl Fig. 4A, B). This suggests that C3G may directly regulate *Fgf1* expression in MKs, which may contribute to the expansion of the adipocyte population in the BM. Similar correlations were observed for *Igf1* (Suppl Fig. 4D) and *Pref1* (Suppl Fig. 4F), in the C3G^{Pf4}-KO model, but not in the transgenic model (Suppl Fig. 4C, E). In contrast, a negative correlation between *Rapgef1* and *Il6* expression was observed (Suppl Fig. 4G, H), along with a significant reduction in *Il6* mRNA levels in tgC3G^{Pf4} MKs (Fig. 2R). These results align with the decreased levels of IL-6 cytokine detected in 5-FU-treated tgC3G^{Pf4} BM (Fig. 2I).

To further evaluate the potential contribution of FGF1 to the role of MK C3G in adipogenesis, we treated HSPCs/MKs from wtC3G^{Pf4} and tgC3G^{Pf4} mice with suramin, able to block the action of factors released by TPO-differentiated Lin^{-} cells. As shown in Fig. 2T, U and Suppl Fig. 3J, suramin completely inhibited the increase in lipid synthesis induced by both wtC3G^{Pf4} and tgC3G^{Pf4} MKs, suggesting the involvement of factors released by MKs. Next, we specifically examined the impact of FGF1 by inhibiting FGF receptor family with infigratinib on 3T3-L1 cells and found that it abrogated the enhanced lipogenesis induced by transgenic C3G expression (Fig. 2T, U and Suppl Fig. 3J). These results strongly support the notion that C3G regulates MK secretion of factors directly involved in adipogenesis, with FGF1 likely playing a key role.

Several transcription factors (e.g. C/EBPα, β γ and PPARγ and other regulatory signals (e.g. Pref-1 and Adiponectin) are known to orchestrate the terminal differentiation of pre-adipocytes into mature adipocytes [50] (Suppl Fig. 5A). We examined whether the expression of any of these regulators was affected in our 2-day co-cultures (day 6 of differentiation). As shown in Suppl Fig. 5B–G, insulin induced the expression of all tested genes in control 3T3-L1 cells. Interestingly, MKs from all genotypes also induced the expression of these genes at levels comparable to insulin. Although not statistically significant, HSPCs/MKs from tgC3G^{Pf4} mice promoted the expression of the terminal differentiation genes *Cebpa* (Suppl Fig. 5E), *Pparg* (Suppl Fig. 5F), and *Adipoq* (Suppl Fig. 5G), at least in the insulin condition, indicating enhanced adipocyte differentiation. This expression pattern aligns with the increased number (Fig. 2M and Suppl Fig. 3C) and signal intensity (Fig. 2L) of lipid droplets, their larger size (Suppl Fig. 3D, H), and the larger size of adipocytes (Fig. 2D) influenced by cues from tgC3G^{Pf4} MKs.

Interestingly, *Pref1* gene expression was notably elevated in 3T3-L1 cells co-cultured with HSPCs/MKs, even in the absence of insulin (MM medium), with levels comparable to those seen in the insulin-containing (DM-II) condition (Suppl Fig. 5D). Among the early genes assessed, *Pref1* is the only one encoding a protein that negatively regulates adipocyte differentiation when secreted [51]. Its persistent expression at this late stage (days 6 of differentiation) is, therefore, intriguing, although it could explain the reduced BODIPY™ intensity observed in the tgC3G^{Pf4} + insulin condition (Suppl Fig. 3B) and the lower number of lipid droplets in MK-co-cultured 3T3-L1 cells compared to controls on day 8 (Suppl Fig. 3G). However, it is important to note that only the secreted form of Pref-1 appears to inhibit adipocyte differentiation [52].

Taking together, these data indicate that MK C3G promotes BMA expansion and maturation, which could contribute to HSPC mobilization following myeloablation.

C3G overexpression in MKs promotes myeloid lineage expansion following 5-FU treatment, while C3G deletion favors CLP accumulation

Our data indicate that C3G levels in MKs influence the amounts of MKs and BMAs in the BM. Given that both cell types function as BM niche cells, we hypothesize that changes in MK C3G expression may affect the HSPC pool during recovery from 5-FU treatment. Although no significant differences in BM cellularity were observed between C3G-modified mice and their corresponding wild-type controls (Fig. 3A, B), we found significant changes in the relative proportions of specific subpopulations during the mid-recovery phase (days 7 and 10) (Fig. 3 and Suppl Figs. 6, 7). Specifically, LKS cells (but not LKS^{-}) were reduced on day 7 in tgC3G^{Pf4} mice

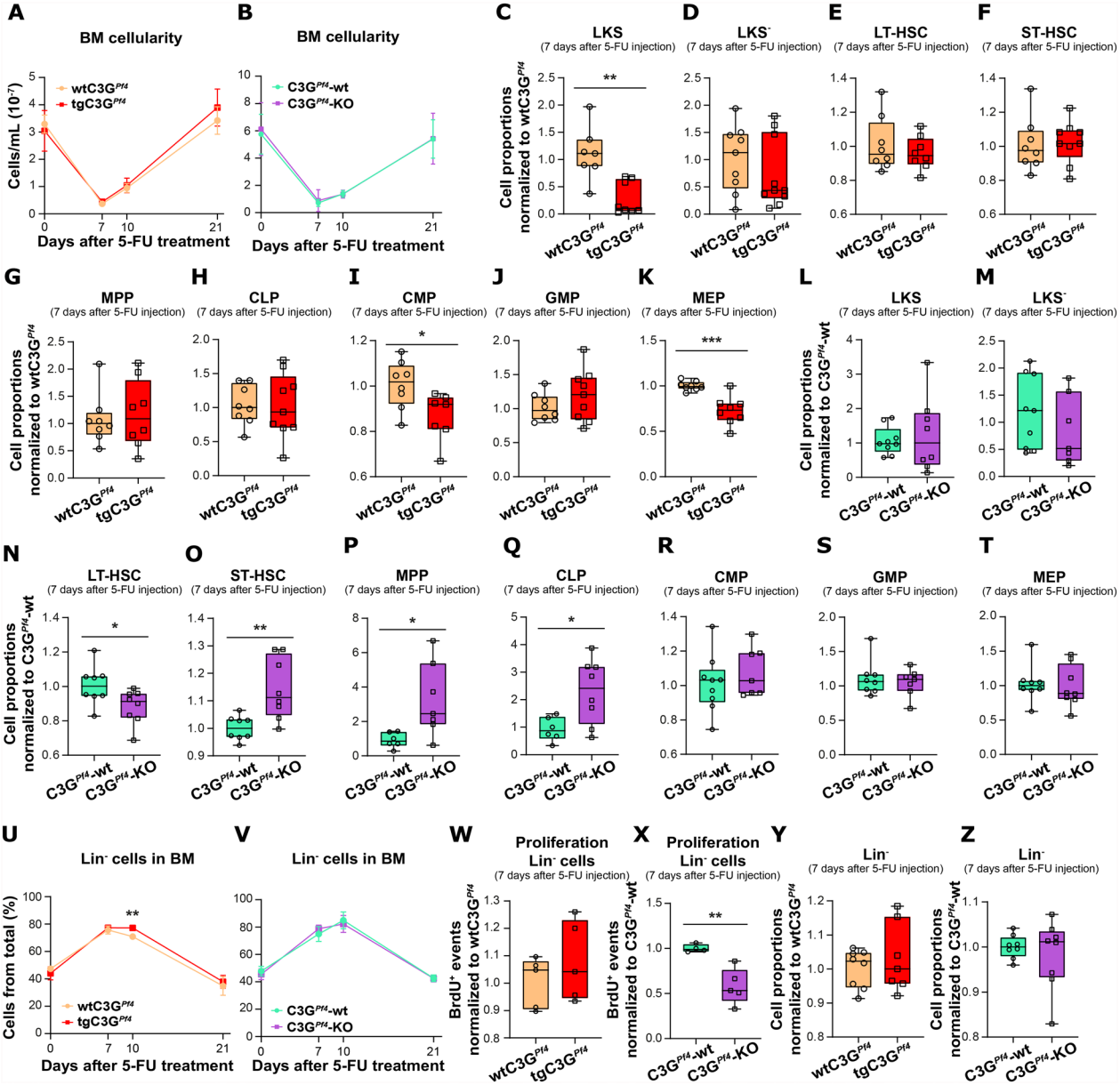

Fig. 3 MK C3G regulates the mobilization of progenitors following 5-FU treatment (**A**, **B**) BM cellularity is depicted as the mean ± SEM of cells from one femur and one tibia of (**A**) wtC3G^{Pf4} and tgC3G^{Pf4} or (**B**) C3G^{Pf4}-wt and C3G^{Pf4}-KO mice throughout the recovery after 5-FU injection. Box plots depict the median and range of (**C**, **L**) LKS, (**D**, **M**) LKS^{-}, (**E**, **N**) LT-HSC, (**F**, **O**) ST-HSC, (**G**, **P**) MPP, (**H**, **Q**) CLP, (**I**, **R**) CMP, (**J**, **S**) GMP, (**K**, **T**) MEP and (**Y**, **Z**) Lin^{-} subpopulations of HSPCs in the BM of tgC3G^{Pf4} or C3G^{Pf4}-KO mice (as indicated) compared to their corresponding wild-type littermates 7 days after 5-FU administration. The values correspond to the proportion within each corresponding parent gate and are normalized to the corresponding wild-types. (**U**, **V**) Percentage of Lin^{-} cells in BM (mean ± SEM) from (**U**) wtC3G^{Pf4} and tgC3G^{Pf4} or (**V**) C3G^{Pf4}-wt and C3G^{Pf4}-KO mice during the 21-day assessment period. (**W**, **X**) Box plots depict the median value and range of the BrdU^{+} Lin^{-} cells from (**W**) tgC3G^{Pf4} mice and (**X**) C3G^{Pf4}-KO mice normalized against their controls, 7 days after the injection of 5-FU. Two independent experiments were performed. Statistics were performed using two-way ANOVA with uncorrected Fisher's LSD post-hoc test in (**A**, **B**, **U**, **V**), and using *t*-test in (**C**–**T**, **W**–**Z**). $^{*}p \le 0.05$. $^{**}p \le 0.01$. $^{***}p \le 0.001$. Three independent experiments were performed

(Fig. 3C, D), although none of its subpopulations (i.e., LT-HSCs, ST-HSCs, MPPs, and CLPs, (see Abbreviations Section)) were proportionally altered (Fig. 3E–H). However, there was a significant reduction in CMP and MEP populations (Fig. 3I, K), accompanied by a slight increase in the GMP population (Fig. 3J). These results, along with the reduced number of MKs (Fig. 1J), the exacerbated platelet rebound (Fig. 1B), and the increased

RBCs (Fig. 1E, F), suggest that C3G-overexpressing MKs induce the mobilization of HSPCs and promote the myeloid branch of hematopoiesis, particularly the MK-erythrocyte lineage.

In contrast, C3G deletion in MKs did not lead to any changes in the LKS or LKS$^-$ populations (Fig. 3L, M) nor in MK-biased progenitors (Fig. 3R, T). However, there was a decrease in the LT-HSC compartment (Fig. 3N), while the ST-HSC (Fig. 3O), MPP (Fig. 3P), and CLP (Fig. 3Q) populations increased proportionally 7 days after 5-FU injection, with no changes in GMPs (Fig. 3S). This, along with the reduced number of WBCs (Fig. 1G), suggests that C3G deletion in MKs promotes HSPC bias toward the lymphoid lineage but impairs their terminal differentiation. No alterations in hematopoiesis due to changes in MK C3G expression were observed in untreated mice (Suppl Fig. 6).

Moreover, while the Lin$^-$ progenitor cell compartment remained significantly increased on day 10 in tgC3G^{Pf4} mice compared to wtC3G^{Pf4} (Fig. 3U and Suppl Fig. 7A), C3G^{Pf4}-KO mice showed a slight decline in this population by day 10 relative to their controls (Fig. 3V and Suppl Fig. 7K). In agreement, the proliferative capacity of C3G^{Pf4}-KO Lin$^-$ cells was reduced on day 7 compared to those from C3G^{Pf4}-wt mice (Fig. 3X), which may explain the population decrease observed 3 days later. Conversely, the proliferative capacity of tgC3G^{Pf4} Lin$^-$ cells was increased, albeit not significantly (Fig. 3W), consistent with the higher number of immature cells noted on day 10 (Suppl Fig. 7A). These tendencies were already noticed on day 7 (Fig. 3Y, Z). In both scenarios, the Lin$^-$ population returned to baseline levels by day 21 (Suppl Fig. 8A–K), along with the other populations (Suppl Fig. 8).

Collectively, these data suggest that MK C3G promotes the proliferation and mobilization of HSPCs, favoring the myeloid branch of hematopoiesis after 5-FU administration, which leads to an increased presence of platelets and erythrocytes in the blood. In contrast, C3G ablation promotes the lymphoid branch.

Altered C3G levels in MKs lead to changes in the levels of mature neutrophils and T-lymphocytes

Next, we explored whether the changes in hematopoietic progenitor populations influenced by MK C3G expression, following 5-FU treatment, extended to mature differentiated cells. Notably, both C3G overexpression (Fig. 4A) and deletion (Fig. 4B) led to an increased percentage of neutrophils under steady-state conditions, which persisted on day 3 in tgC3G^{Pf4} mice. An increase in neutrophil counts in PB has previously been reported in tgC3G^{Pf4} mice [2]. During recovery from neutrophil depletion, C3G^{Pf4}-KO mice exhibited an increase in neutrophils, while tgC3G^{Pf4} mice showed a decrease, in line with a role for C3G in promoting megakaryopoiesis. No significant changes were observed in the percentage of T lymphocytes in the PB of tgC3G^{Pf4} mice (Fig. 4C). However, between days 7 and 14, the proportion of CD4$^+$ and CD8$^+$ cells shifted in favor of the latter (Fig. 4D, E). Consistently, a bias toward the CD4$^+$ phenotype was observed within the CD3$^+$ lymphocyte population of C3G^{Pf4}-KO mice compared to their C3G^{Pf4}-wt counterparts (Fig. 4G, H) with no significant changes in CD3$^+$ cell expansion (Fig. 4F). No changes in B cell number were observed in tgC3G^{Pf4} mice (Fig. 4I); however, a slight increase was noted in C3G^{Pf4}-KO mice (Fig. 4J).

These findings suggest that MK C3G alters blood cell population percentages, likely by promoting a shift towards the MK-platelet and erythrocyte lineages following BM depletion, consistent with the results shown in Figs. 1 and 3.

C3G deletion prevents 5-FU associated splenomegaly

5-FU administration induces EMH, leading to splenomegaly [24]. To assess EMH in our models, spleens were harvested at three time points: before treatment (day 0), at mid-recovery (day 7), and after recovery (day 21). As expected, 5-FU administration resulted in splenomegaly on day 21 in both control and tgC3G^{Pf4} mice (Fig. 4K), reflecting the spleen supportive role in hematopoietic recovery following myeloablation. However, C3G^{Pf4}-KO mice did not develop splenomegaly compared to untreated mice (Fig. 4L). This suggests that MKs are involved in 5-FU-induced EMH, and that C3G is critical for this MK function.

C3G exerts a protective role in recovery following repeated cycles of 5-FU, but only in female mice

The data in Fig. 1B, D, E, together with the increased precursor mobilization shown in Fig. 3C, I, K, suggest that C3G overexpression in MKs accelerates the recovery of blood cell populations following 5-FU-induced myeloablation, while C3G^{Pf4}-KO mice exhibited a delayed recovery (Figs. 1C–G and 3O–Q). To investigate this further, mice were subjected to consecutive weekly cycles of 5-FU and their survival was analyzed (Fig. 5A). Altering C3G levels in MKs significantly impacted survival, but only in female mice (Fig. 5B–G). Specifically, female tgC3G^{Pf4} mice survived an average of 3.5 days longer than their wild-type littermates (Fig. 5C), whereas C3G deletion resulted in a 1-day reduction in survival (Fig. 5F). These findings are consistent with the enhanced proliferative capacity of progenitor cells in tgC3G^{Pf4} mice and the reduced capacity in C3G^{Pf4}-KO mice (Fig. 3W, X), further supporting a positive role for MK C3G in hematopoietic recovery following myeloablation.

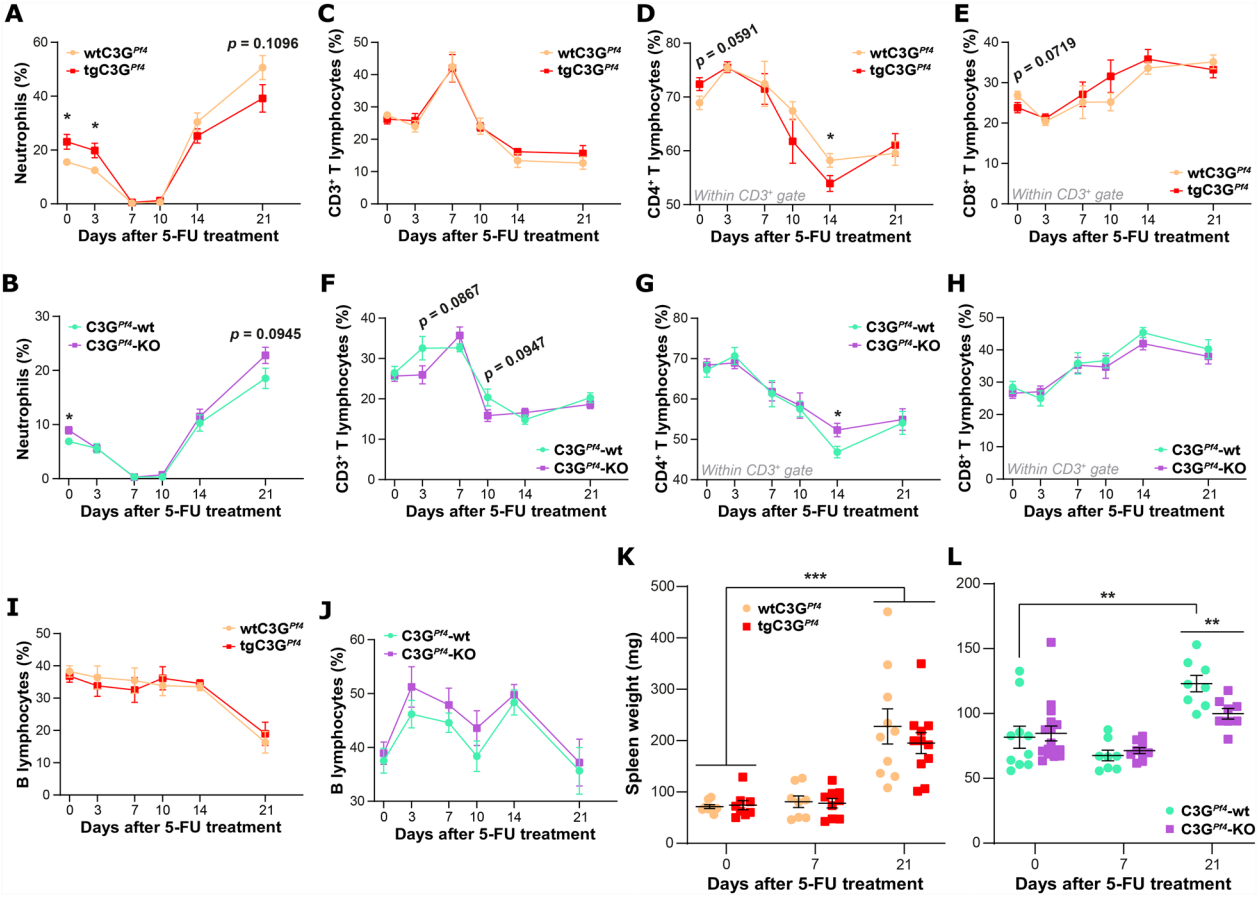

Fig. 4 MK C3G regulates the levels of mature neutrophils and T-lymphocytes after 5-FU-induced myeloablation XY plots display the mean ± SEM of the percentage of (**A**, **B**) neutrophils, (**C**–**H**) T lymphocytes and (**I**, **J**) B lymphocytes in (**A**, **C**–**E**, **I**) wtC3G^{Pf4} and tgC3G^{Pf4} or (**B**, **F**–**H**, **J**) C3G^{Pf4}-wt and C3G^{Pf4}-KO PB during the 21-day recovery period after 5-FU administration. Percentages shown in (**D**, **E**, **G**, **H**) are those within the CD3$^+$ T lymphocyte gate. Five independent experiments were performed. wtC3G^{Pf4}, n = 11; tgC3G^{Pf4}, n = 13; C3G^{Pf4}-wt, n = 14; C3G^{Pf4}-KO, n = 14. (**K**, **L**) Interleaved scatter plots display the mean ± SEM of spleen weight of either (**K**) tgC3G^{Pf4} or (**L**) C3G^{Pf4} KO mice, as well as their corresponding wild-type siblings at the indicated time points following 5-FU administration. Three to five independent experiments were performed per day of analysis. Statistical analysis was performed using two-way ANOVA with uncorrected Fisher's LSD post-hoc test. *$p \le 0.05$; **$p \le 0.01$; ***$p \le 0.001$

C3G modulates the expression of genes affecting HSCs in MKs

To further investigate the mechanism by which C3G levels in MKs influence HSPC fate, we examined whether C3G affects the expression of key MK genes known to modulate HSPCs, specifically *Tpo*, *Pf4*, *Sdf1*, and *Tgfb1* (Fig. 5H–K and Suppl Fig. 4I–P), in addition to the previously analyzed *Il6* (Fig. 2R and Suppl Fig. 4G, H). In C3G^{Pf4}-KO MKs *Tpo* and *Tgfb1* expression was reduced (Fig. 5H, K), consistent with the diminished thrombopoiesis observed in C3G^{Pf4}-KO mice (Fig. 1C) and in previous studies [3, 53]. *Pf4*, which is associated with a reduced number of HSCs and increased quiescence [54], also exhibited a trend toward lower expression in C3G-deficient MKs (Fig. 5I). Similarly, SDF1, a chemokine involved in HSPC quiescence and MK migration [55], followed the same pattern (Fig. 5J). This indicates that C3G might play a role in promoting MK-induced HSC quiescence in the absence of external stimuli. This observation is further supported by the elevated *Sdf1* mRNA expression in MKs lacking the Rap1 GAP Sipa-1 (Suppl Fig. 9A), which also regulates the BM niche [36]. *Il6* expression was also increased in Sipa1-KO MKs (Suppl Fig. 9B), consistent with the involvement of both IL-6 and the Rap1 signaling pathway in myeloid differentiation [56, 57]. In contrast, C3G overexpression led to decreased *Il6* mRNA levels in MKs (Fig. 2R), which supports the better recovery of these mice, since IL-6 is known to play an inhibitory role in the early stages of megakaryopoiesis [58]. A correlation between *C3G* expression and *Tpo* expression was observed in C3G^{Pf4}-KO mice (Suppl Fig. 4J), but not in tgC3G^{Pf4} mice (Suppl Fig. 4I). Similarly, *Rapgef1* expression correlated with *Pf4* expression in C3G^{Pf4}-KO

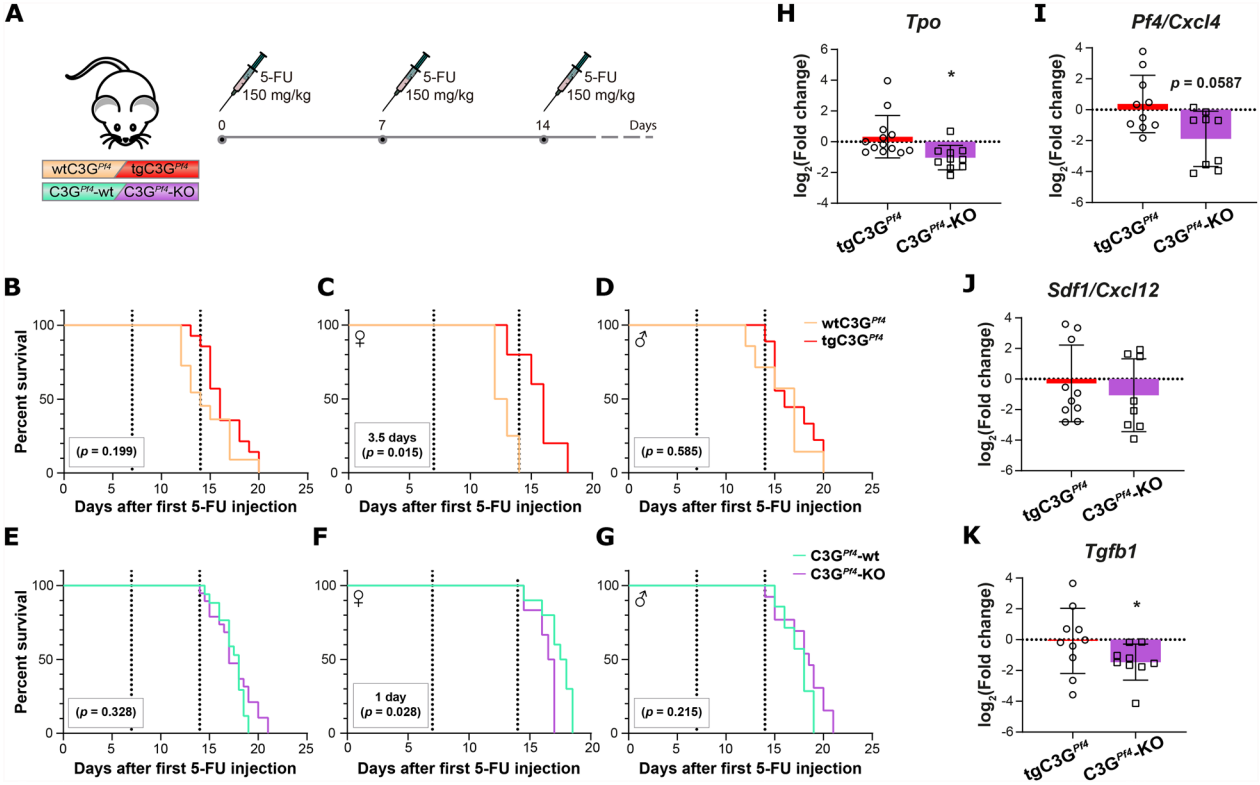

Fig. 5 Overexpression of C3G in MKs enhances the survival of female mice following weekly 5-FU administration (**A**) Scheme illustrating the 5-FU administration schedule for the 5-FU challenge. Kaplan-Meyer curves depict the overall survival of mice after repeated weekly administration of 150 mg/kg 5-FU in (**B**–**D**) wtC3G^{Pf4} and tgC3G^{Pf4} mice, and (**E**–**G**) C3G^{Pf4}-wt and C3G^{Pf4}-KO mice. Results are shown for (**B**, **E**) all the mice tested, (**C**, **F**) only females and (**D**, **G**) only males. The first injection was performed on day 0. Each additional dose is represented as a dotted line in the plot. The difference in median survival and *p*-value according to the Log-rank (Mantel-Cox) test are shown in the squared box. Five to six independent experiments were performed. wtC3G^{Pf4}, n = 11 (4 females, 7 males); tgC3G^{Pf4}, n = 14 (5 females, 9 males); C3G^{Pf4}-wt, n = 17 (10 females, 7 males); C3G^{Pf4}-KO, n = 19 (6 females, 13 males). (**H**–**K**) Bar plots show the mean ± SEM of the $\log_2$(Fold change) of mRNA expression analyzed by RT-qPCR of (**H**) *Tpo*, (**I**) *Pf4/Cxcl4*, (**J**) *Sdf1/Cxcl12*, and (**K**) *Tgfb1* in CD41$^+$CD42$^+$ MKs isolated from the BM of tgC3G^{Pf4} and C3G^{Pf4}-KO mice, and their corresponding wild-types. Values are relative to β-actin levels and normalized to the corresponding wild-type control. *$p \leq 0.05$

(Suppl Fig. 4L). No correlation was detected in the rest of the conditions (Suppl Fig. 4K, M, N, O, P).

C3G influences the niche function of MKs in a transplant setting

Next, we investigated whether the effects of MK C3G on the HSC population could be observed in different contexts. To this end, we assessed the impact of MK C3G on the recovery of mice subjected to TBI followed by whole bone marrow (WBM) transplantation (Fig. 6A). WBM cells from Ly5.1 mice repopulated PB populations similarly across all host genotypes. However, the percentages were slightly lower in tgC3G^{Pf4} mice compared to wtC3G^{Pf4} controls (Fig. 6B), and higher in C3G^{Pf4}-KO mice (Fig. 6C), particularly at 1 month of age. Indeed, with the exception of B cells, CD45.1$^+$ cells generally contributed equal or less to BM repopulation in tgC3G^{Pf4} mice compared to controls (Fig. 6D–G), consistent with the lower percentage of CD45.1$^+$ cells in tgC3G^{Pf4} BM (Fig. 7A). The opposite trend was observed in C3G^{Pf4}-KO mice compared to their controls for neutrophils, but not for T cells (Fig. 6H–K). Since total BM cellularity nine months after transplantation was similar in wtC3G^{Pf4} and tgC3G^{Pf4} mice (Fig. 7B), cells other than the transplanted ones are contributing to BM repopulation in tgC3G^{Pf4} mice. One potential explanation is that the BM of tgC3G^{Pf4} mice was more resistant to myeloablation than that of wtC3G^{Pf4} mice, which could enhance repopulation, consistent with the results in Fig. 5C. This hypothesis is supported by the lower BM cellularity observed in C3G^{Pf4}-KO mice (Fig. 7D), alongside a similar contribution of CD45.1$^+$ cells compared to C3G^{Pf4}-wt mice (Fig. 7C), indicating that host (CD45.2$^+$) BM cells from C3G^{Pf4}-KO mice may be less resistant to TBI. In addition, the reduced proportions of CD41$^+$, ST-HSC and MPP populations in tgC3G^{Pf4} BM (Fig. 7E, H, I), with no changes in CD41$^+$ and MPP populations in C3G^{Pf4}-KO mice (Fig. 7F, L), indicates that MK C3G may promote

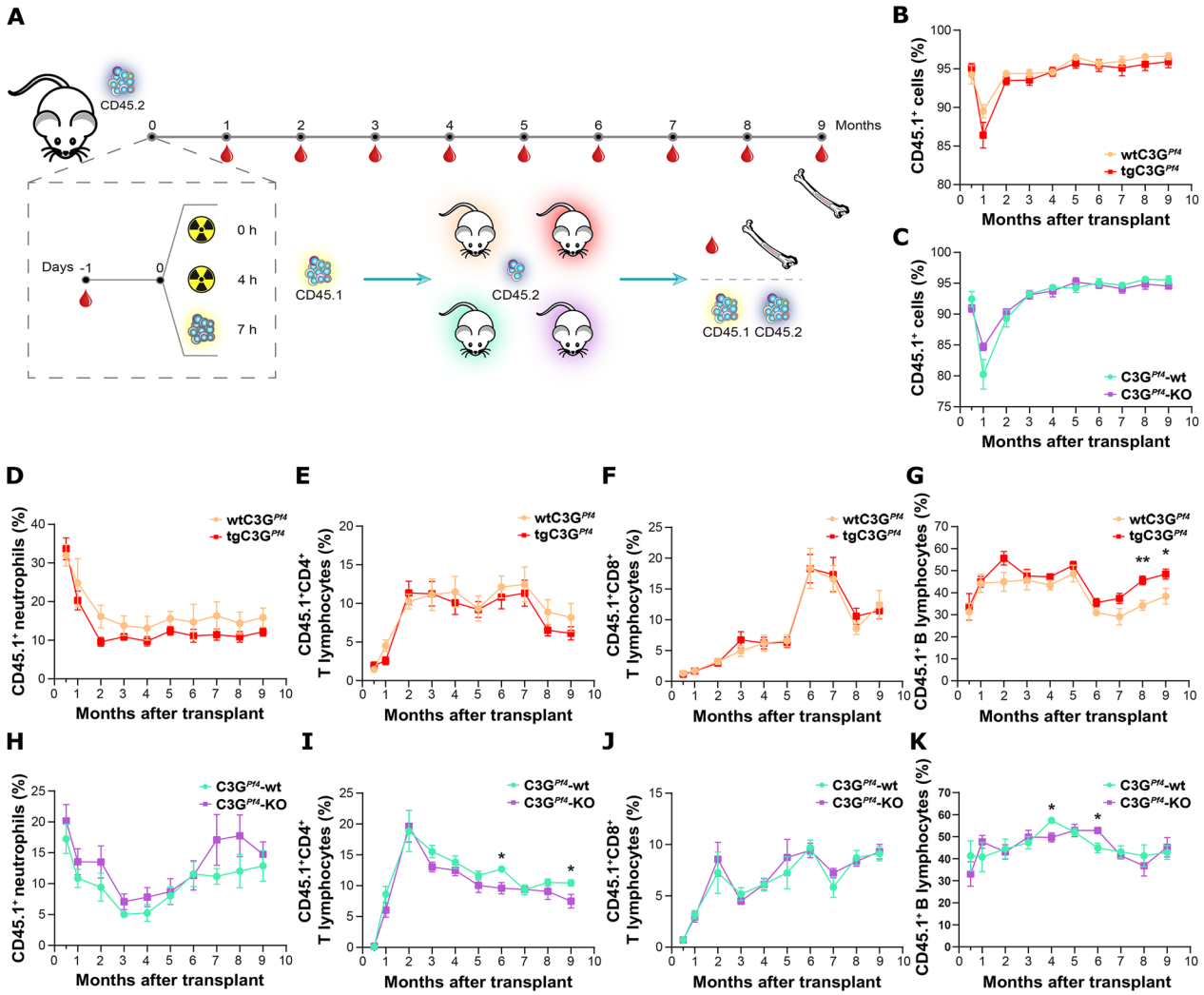

Fig. 6 MK C3G modulates neutrophil and lymphocyte reconstitution after TBI. (**A**) Transplantation setup. Two million BM CD45.1$^+$ cells from a 7- to 10-week old Ly5.1 mouse were transplanted into lethally irradiated wtC3G^{Pf4}, tgC3G^{Pf4}, C3G^{Pf4}-wt and C3G^{Pf4}-KO, recipient mice (CD45.2). PB of the recipients was monitored monthly after transplantation and the BM analyzed at the endpoint of the experiment (9 months, see Fig. 7). XY plots display the mean ± SEM of the assessment of the proportion of donor (CD45.1$^+$) cells evaluated during a 9-month period after transplantation. The percentages of (**B**, **C**) BM cells, (**D**, **H**) neutrophils, (**E**, **I**) CD4$^+$ T lymphocytes, (**F**, **J**) CD8$^+$ T lymphocytes, and (**G**, **K**) B lymphocytes in the PB were analyzed following the transplantation of 2×10^6 WBM cells from Ly5.1 mice into lethally irradiated recipients: either (**B**–**D**–**G**) wtC3G^{Pf4} and tgC3G^{Pf4} or (**C**, **H**–**K**) C3G^{Pf4}-wt and C3G^{Pf4}-KO mice. Statistical analysis was performed using two-way ANOVA with uncorrected Fisher's LSD post-hoc test. *$p \le 0.05$. **$p \le 0.01$. Three independent experiments were performed. wtC3G^{Pf4}, n = 7; tgC3G^{Pf4}, n = 9; C3G^{Pf4}-wt, n = 5; C3G^{Pf4}-KO, n = 6

enhanced mobilization of myeloid/megakaryocytic precursors, consistent with findings from the 5-FU model. Moreover, C3G^{Pf4}-KO animals exhibited an accumulation of the most immature precursors in the BM (Fig. 7J, K) and increased neutrophil counts in PB (Fig. 6H). This suggests impaired MK differentiation, further supporting the hypothesis.

No changes in LT-HSC population were observed in tgC3G^{Pf4} mice (Fig. 7G). Furthermore, the proportions of Lin$^-$ (Fig. 7M, N), LKS (Fig. 7O, P) and LKS$^-$ (Fig. 7Q, R) populations were not affected by C3G overexpression or deletion in MKs. Finally, no alterations in spleen size were noted in any of the recipient mice nine months after transplantation (Suppl Fig. 9C, D).

These results indicate that MK C3G enhances the mobilization of precursor cells biased toward the myeloid/megakaryocytic branch in the bone marrow following transplantation, leading to decreased percentages of lymphocyte and neutrophil populations in PB. This phenotype mirrors that observed in the 5-FU model.

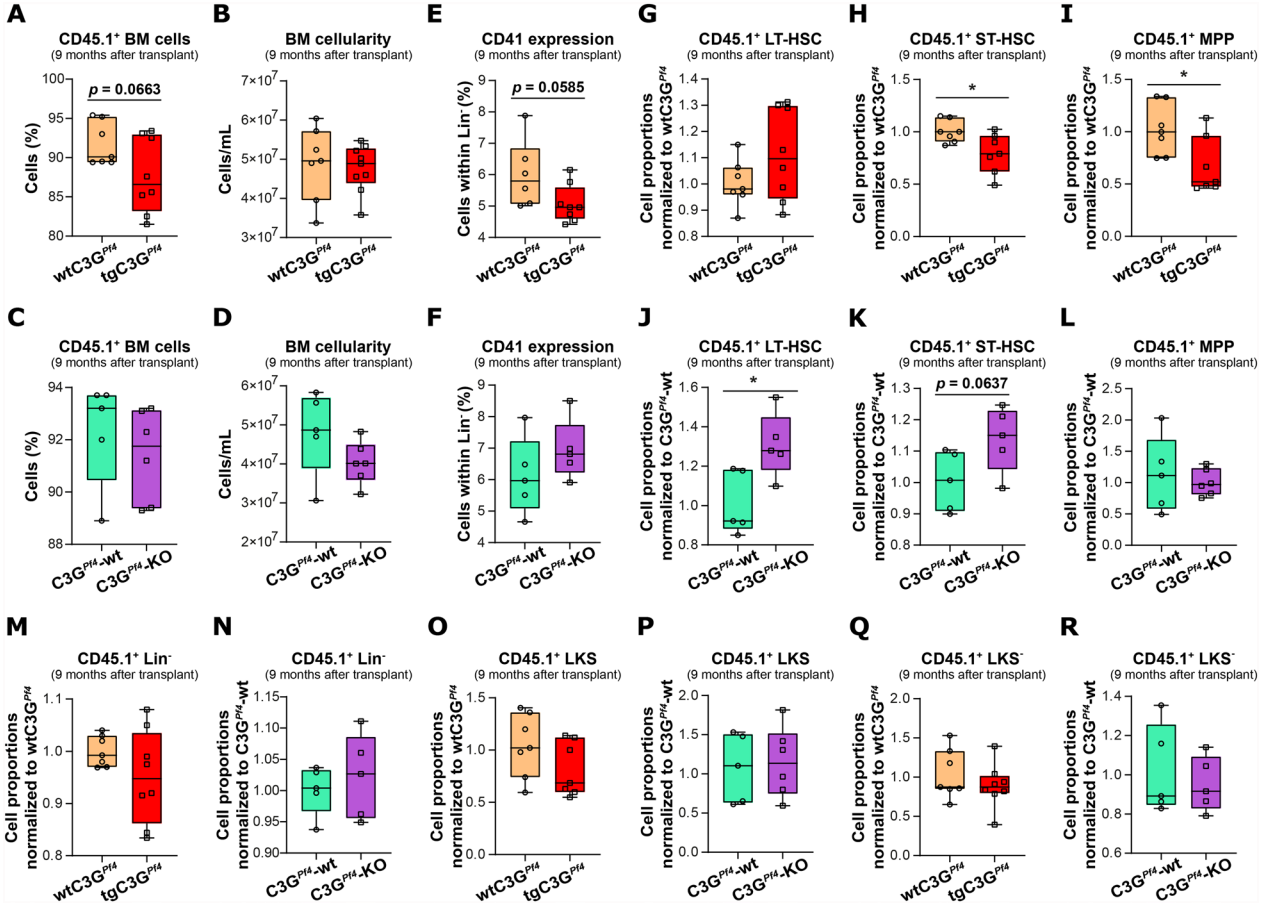

Fig. 7 C3G influences the niche function of MKs in a transplant setting. Box plots depict the median and range of (**A**, **C**) the percentage of donor (CD45.1$^+$) BM cells, (**B**, **D**) total marrow cellularity, (**E**, **F**) CD41-expressing BM cells, (**G**, **J**) LT-HSC, (**H**, **K**) ST-HSC, (**I**, **L**) MPP, (**M, N**) Lin$^-$, (**O**, **P**) LKS and (**Q**, **R**) LKS$^-$ subpopulations of HSPCs in the BM of (**A**, **B**, **E**, **G**, **H**, **I**, **M**, **O**, **Q**) tgC3G^{Pf4} mice or (**C**, **D**, **F**, **J**, **K**, **L**, **N**, **P**, **R**) C3G^{Pf4}-KO mice compared to their corresponding wild-type littermates 9 months after transplantation with a 2×10^6-WBM-cell graft. The proportion values in (**G**–**R**) were normalized to wtC3G^{Pf4} or C3G^{Pf4}-KO, as appropriate. Statistical analyses were performed using *t*-test. *$p \le 0.05$. Three independent experiments were performed

Discussion

In this study, we provide further evidence for the role of C3G in megakaryopoiesis, within the context of 5-FU–induced bone marrow myeloablation, and TBI followed by WBM transplantation, using genetically modified mouse models targeting C3G in MKs. In addition, our data suggest that MK C3G contributes to hematopoietic regeneration and that MKs are involved in BM adipogenesis, with C3G potentially playing a key role in this MK niche function.

Our group has previously demonstrated the significant role of C3G in platelet homeostasis [2, 3, 5], as well as in other platelet-mediated functions, including angiogenesis, tumor growth, metastasis, and the regulation of platelet mass via c-Cbl-mediated TPO endocytosis and degradation [4, 6]. Additionally, we have identified a role for C3G in both megakaryopoiesis and thrombopoiesis after challenging the hematopoietic system with TPO or chemotherapy [6, 8], with our data also suggesting that MK C3G may contribute to bone marrow adipogenesis after melanoma cell implantation [8].

In the 5-FU model, MK C3G facilitated MK maturation and platelet production during recovery, which correlated with a transient decrease in the MK population in the BM, particularly in the diaphysis. Interestingly, MK C3G also enhanced the recovery of WBCs and RBCs, which was associated with increased proliferation of Lin$^-$ cells and mobilization of LKS cells. These findings suggest a potential role for C3G in the niche function of MKs, known to promote HSC proliferation and differentiation after injury [12]. The platelet rebound induced by 5-FU is the result of an indirect effect on BM niche cells, rather than a direct impact on HSCs [59]. Therefore, the involvement of MK C3G in this process, as observed here and previously [6], further supports a key role for C3G in MK function as niche cells within the BM. Furthermore,

C3G expression in MKs positively correlated with *Fgf1* expression, a factor known to promote HSC expansion during 5-FU-induced BM depletion [16].

Despite increased WBC counts in tgC3G^{Pf4} mice, we observed a trend toward lower proportions of neutrophils and CD4^{+} T lymphocytes during recovery, with the opposite trend seen in C3G^{Pf4}-KO mice. This pattern aligns with the observed CMP mobilization and its bias favoring MEP over GMP differentiation. The C3G-driven bias toward megakaryopoiesis over other myeloid lineages is further supported by the decreased *Il6* expression detected in tgC3G^{Pf4} MKs. While IL-6 promotes myeloid lineage differentiation [60], it has a negative impact on the early stages of megakaryopoiesis [58]. This appears to be in contrast with the Sipa1-KO results (Suppl Fig. 9B), which show an increase in *Il6* expression. However, it is important to consider that Sipa1-KO is a systemic knock-out [7], which could explain the observed differences.

On the other hand, C3G ablation in MKs led to an accumulation of progenitors primarily within the lymphoid branch. C3G deletion favored CLP production, but appeared to block their progression to mature lymphocytes, suggesting a role for MK C3G in lymphocyte maturation. Consistent with this, previous studies have reported a role for C3G-Rap1 signaling in T-cell homeostasis and function [61, 62]. Our data also indicate an essential role for MK C3G in EMH following 5-FU treatment, as evidenced by the absence of splenomegaly in C3G^{Pf4}-KO animals.

In parallel, MK C3G altered the adipokine content of the BM (Fig. 2I), promoting an enrichment in mature BMAs, accompanied by a reduction in APCs. This MK C3G-mediated increase in BMAs following a stress stimulus aligns with previous findings [8] and suggests a potential role for MK C3G in regulating adipogenesis. Our in vitro results further corroborate this, demonstrating that MKs promote the adipocytic differentiation of 3T3-L1 cells, with C3G likely enhancing this process by modulating the expression of MK-derived factors involved in adipogenesis. Specifically, C3G positively modulated the expression of *Fgf1*, *Igf1*, *Pref1*, and negatively that of *Il6* in MKs, all of which are relevant regulators of adipogenesis [31–34]. Interestingly, the reduced ability of tgC3G^{Pf4} HSPCs/MKs to promote adipogenesis following selective FGFR inhibition (Fig. 2S–U, Suppl Fig. 3J), postulates FGF1 as a key factor in MK C3G-mediated adipocyte expansion in the BM after myeloablation. Although the secreted form of Pref-1 can act as a negative regulator of adipogenesis [52], the effect of membrane-bound Pref-1 remains unclear. Furthermore, a hierarchical relationship exists among these factors, such that the presence of IGF1 supersedes Pref-1 [63]. This hierarchy, along with the complexity of Pref-1 effect, may explain how C3G overexpression promotes adipogenesis despite elevated *Pref1* mRNA levels. On the other hand, there was neither a synergistic nor additive effect between MK cues and insulin on the expression of adipocyte late differentiation genes. However, factors from C3G-overexpressing MKs appeared to enhance the insulin response, consistent with C3G role in regulating platelet secretion [5].

Other studies have established a relationship between MKs and BMAs. Specifically, adipocytes enhance megakaryopoiesis by promoting MK polyploidization and proplatelet formation through fatty acid transfer from adipocytes to MKs via CD36 translocase. MKs may then create a positive feedback loop by inducing delipidation of adipocytes, likely mediated by MK releasate [29, 30]. However, to our knowledge, this is the first report identifying a role for MKs in BM adipogenesis, highlighting the significant contribution of C3G.

The effect of MK C3G on HSC proliferation and differentiation after injury may also be indirectly linked to its influence on BMAs, which are known to promote hematopoiesis in response to stress stimuli [26, 27]. Yet, in the absence of stimuli, C3G appears to promote MK-induced HSC quiescence by modulating *Tpo*, *Pf4*, and *Sdf1* expression. Notably, the expression of *Tpo* in MKs correlates with that of *Rapgef1*, further supporting the involvement of C3G in megakaryopoiesis and thrombopoiesis. As previously noted, our group has demonstrated that the regulation of platelet secretion is likely the most critical function of C3G in platelet biology. C3G regulates actin remodeling and trans-SNARE complex formation through mechanisms involving PKCδ, RalA-Rap1, and Rac1 pathways [5]. This, combined with the observation that MKs influence BMAs without requiring direct contact, strongly supports the hypothesis that C3G acts as a key regulator of MK secretion.

The positive effect of C3G on BM recovery after depletion is further evidenced by the increased survival observed in tgC3G^{Pf4} female mice and the decreased survival seen in C3G^{Pf4}-KO female mice. Some studies suggest that certain signaling pathways involving C3G could influence metabolic conditions differently in males and females due to broader hormonal and genetic interactions. For instance, polymorphisms in the *Rapgef1* gene have been associated with diabetes [64, 65], a condition globally more prevalent in women than in men [66]. Additionally, *Rapgef1* polymorphisms have been linked to persistent lactation and mastitis in dairy cows [67], and the *Rapgef1* promoter has been found demethylated in gynecological cancers [68]. However, direct research confirming gender-specific effects of C3G remains limited.

In the transplantation model, although tgC3G^{Pf4} mice showed a slightly reduced contribution of CD45.1^{+} cells to hematopoiesis nine months post-transplantation, our results indicate increased mobilization of hematopoietic precursors due to MK C3G overexpression, particularly of CD41^{+} cells. As with the 5-FU model, this finding suggests a C3G-mediated differentiation of MK-primed progenitors. Consistently, C3G ablation in MKs led to reduced progenitor mobilization. The reduced number of CD45.1^{+} cells in the BM of tgC3G^{Pf4} mice may be attributed to several factors: (i) poorer engraftment influenced by the MK C3G niche, and/or (ii) greater resistance of the tgC3G^{Pf4} niche to irradiation, mediated by MK C3G, resulting in a lower proportion of CD45.1^{+} cells. In the first scenario, one possible explanation is an increased BMA population due to MK C3G, which is known to negatively impact BM engraftment post-transplant [25]. However, as previously discussed, BMA abundance may also have a positive effect on HSC proliferation following irradiation or chemotherapy [27, 28], making both scenarios plausible.

Conclusions

In conclusion, our findings highlight a novel role for C3G as a key factor in the niche function of MKs during BM recovery following chemotherapy or transplantation. Moreover, we reveal that MKs are significant regulators of BM adipogenesis during this process, with C3G playing a crucial role by promoting the release of FGF1 and potentially other factors from MKs that alter the adipokine content of the BM. Hence, the enhanced hematopoietic regeneration observed in the tgC3G^{Pf4} model is likely due to increased secretion by mature MKs and, potentially, the indirect effects of elevated BM adipocytes. These insights not only deepen our understanding of BM recovery mechanisms but also underscore the potential for targeting C3G in therapeutic strategies aimed at enhancing hematopoietic reconstitution and improving outcomes in chemotherapy-treated and transplanted patients.

Abbreviations

5-FU	5-Fluorouracil
APC	Adipocyte progenitor cell
BM	Bone marrow
BMA	Bone marrow adipocyte
BMAT	Bone marrow adipose tissue
BMT	Bone marrow transplantation
CLP	Common lymphoid progenitor
CMP	Common myeloid progenitor
EMH	Extramedullary hematopoiesis
FACS	Fluorescence-activated cell sorting
GAP	GTPase activating protein
GEF	Guanine nucleotide exchange factor
GMP	Granulocyte/monocyte progenitor
HSC	Hematopoietic stem cell
HSPC	Hematopoietic stem and progenitor cell
KO	Knock-out
Lin	Lineage
LT-HSC	Long-term hematopoietic stem cell
MACS	Magnetic-activated cell sorting
MAT	Marrow adipose tissue
MEP	Megakaryocyte/erythrocyte progenitor
MK	Megakaryocyte
MPP	Multipotent progenitor
MSC	Mesenchymal stem cell
PB	Peripheral blood
PF4	Platelet factor 4
RBC	Red blood cell
ST-HSC	Short-term hematopoietic stem cell
TBI	Total body irradiation
TPO	Thrombopoietin
WBC	White blood cell
WBM	Whole bone marrow

Supplementary Information

The online version contains supplementary material available at https://doi.org/10.1186/s13045-025-01687-1.

Supplementary material 1

Acknowledgements

We thank Dr. Hong Qian (Karolinska University Hospital, Stockholm, Sweden) for her support in the studies with the Sipa1-KO mouse model. We also acknowledge the Mouse Model Experimentation Unit (CIC, Salamanca, Spain) for their assistance with the mouse colonies, as well as the Pathology Service and the Microscopy and Cytometry Services at CIC for their technical assistance.

Author contributions

ÓH and CG designed the research; ÓH performed most of the experiments and analyzed the data; PB helped with the transplant experiments; CS-N contributed to the analysis of progenitors by flow cytometry; CF-I and LH-C performed the gene expression analysis; ÓH and CG interpret the data and wrote the paper; AP contributed to data interpretation and critically reviewed the manuscript; CG and AP were responsible for the acquisition of funding. All authors read and approved the submitted version of the manuscript.

Funding

This work was supported by grants PID 2019-104143RB-C21 and PID2022-137717OB-C22 (CG), PID 2019-104143RB-C22 and PID2022-137717OB-C21 (AP) funded by MCIN/AEI/10.13039/501100011033 and ERDF "A way of making Europe", and by grant SA078P20 (CG) funded by the Council of Education of Junta de Castilla y León, Spain and ERDF "A way of making Europe". ÓH and CS-N are recipients of FPU fellowships from the Spanish Ministry of Education. PB, CF-I and LH-C are recipients of fellowships from the Council of Education of Junta de Castilla y León, Spain, and The Social European Funding. ÓH was also recipient of an EMBO Scientific Exchange Grant. The authors' institution is supported by the Programa de Apoyo a Planes Estratégicos de Investigación de Estructuras de Investigación de Excelencia co-funded by Junta de Castilla y León and ERDF (CLC-2017–01) and by the Scientific Foundation of the Spanish Association Against Cancer (Programa Excelencia 2022 EPAEC222641CICS).

Availability of data and materials

Data and further details regarding the manuscript are available from the corresponding author on reasonable request.

Declarations

Ethics approval and consent to participate

This study has been reviewed and approved by The Committee on the Ethics of Animal Experiments of the University of Salamanca and the Department of Agriculture, Livestock and Rural Development, Regional Government of Castilla y León, Spain (project reference: 639). All experiments were carried out in

strict accordance with the guidelines described in the EU Directive 2010/63/EU for animal experimentation, including the "three R's" rule, and every effort was made to minimize suffering.

Consent for publication
Not applicable.

Competing interests
The authors declare that they have no competing interests.

Received: 29 November 2024 Accepted: 11 March 2025
Published online: 01 April 2025

References

1. Popovic M, Rensen-de Leeuw M, Rehmann H. Selectivity of CDC25 homology domain-containing guanine nucleotide exchange factors. J Mol Biol. 2013;425(15):2782–94.
2. Gutiérrez-Herrero S, Maia V, Gutiérrez-Berzal J, Calzada N, Sanz M, González-Manchón C, et al. C3G transgenic mouse models with specific expression in platelets reveal a new role for C3G in platelet clotting through its GEF activity. Biochim Biophys Acta Mol Cell Res. 2012;1823(8):1366–77.
3. Gutiérrez-Herrero S, Fernandez-Infante C, Hernandez-Cano L, Ortiz-Rivero S, Guijas C, Martin-Granado V, et al. C3G contributes to platelet activation and aggregation by regulating major signaling pathways. Signal Transduct Target Ther. 2020;5:29.
4. Martín-Granado V, Ortiz-Rivero S, Carmona R, Gutiérrez-Herrero S, Barrera M, San-Segundo L, et al. C3G promotes a selective release of angiogenic factors from activated mouse platelets to regulate angiogenesis and tumor metastasis. Oncotarget. 2017;8(67):110994–1011.
5. Fernández-Infante C, Hernández-Cano L, Herranz O, Berrocal P, Sicilia-Navarro C, González-Porras JR, et al. Platelet C3G: a key player in vesicle exocytosis, spreading and clot retraction. Cell Mol Life Sci. 2024;81(1):84.
6. Hernández-Cano L, Fernández-Infante C, Herranz O, Berrocal P, Lozano FS, Sánchez-Martín MA, et al. New functions of C3G in platelet biology: contribution to ischemia-induced angiogenesis, tumor metastasis and TPO clearance. Front Cell Dev Biol. 2022;10:1026287.
7. Ishida D, Kometani K, Yang H, Kakugawa K, Masuda K, Iwai K, et al. Myeloproliferative stem cell disorders by deregulated Rap1 activation in SPA-1-deficient mice. Cancer Cell. 2003;4:55–65.
8. Ortiz-Rivero S, Baquero C, Hernandez-Cano L, Roldan-Etcheverry JJ, Gutierrez-Herrero S, Fernandez-Infante C, et al. C3G, through its GEF activity, induces megakaryocytic differentiation and proplatelet formation. Cell Commun Signal. 2018;16(1):101.
9. Radha V, Mitra A, Dayma K, Sasikumar K. Signalling to actin: role of C3G, a multitasking guanine-nucleotide-exchange factor. Biosci Rep. 2011;31(4):231–44.
10. Vishnu VV, Muralikrishna B, Verma A, Nayak SC, Sowpati DT, Radha V, et al. C3G regulates STAT3, ERK, Adhesion signaling, and is essential for differentiation of embryonic stem cells. Stem Cell Rev Rep. 2021;17(4):1465–77.
11. Palao N, Sequera C, Cuesta AM, Baquero C, Bragado P, Gutierrez-Uzquiza A, et al. C3G down-regulation enhances pro-migratory and stemness properties of oval cells by promoting an epithelial-mesenchymal-like process. Int J Biol Sci. 2022;18(15):5873–84.
12. Zhao M, Perry JM, Marshall H, Venkatraman A, Qian P, He XC, et al. Megakaryocytes maintain homeostatic quiescence and promote post-injury regeneration of hematopoietic stem cells. Nat Med. 2014;20(11):1321–6.
13. Zhan H, Kaushansky K. Megakaryocytes as the Regulator of the Hematopoietic Vascular Niche. Front Oncol. 2022;12: 912060.
14. Crane GM, Jeffery E, Morrison SJ. Adult haematopoietic stem cell niches. Nat Rev Immunol. 2017;17(9):573–90.
15. Qian H, Buza-Vidas N, Hyland CD, Jensen CT, Antonchuk J, Mansson R, et al. Critical role of thrombopoietin in maintaining adult quiescent hematopoietic stem cells. Cell Stem Cell. 2007;1(6):671–84.
16. Batsivari A, Haltalli MLR, Passaro D, Pospori C, Lo Celso C, Bonnet D. Dynamic responses of the haematopoietic stem cell niche to diverse stresses. Nat Cell Biol. 2020;22(1):7–17.
17. Purton LE. Adult murine hematopoietic stem cells and progenitors: an update on their identities, functions, and assays. Exp Hematol. 2022;116:1–14.
18. Noetzli LJ, French SL, Machlus KR. New insights into the differentiation of megakaryocytes from hematopoietic progenitors. Arterioscler Thromb Vasc Biol. 2019;39(7):1288–300.
19. Mendez-Ferrer S, Bonnet D, Steensma DP, Hasserjian RP, Ghobrial IM, Gribben JG, et al. Bone marrow niches in haematological malignancies. Nat Rev Cancer. 2020;20(5):285–98.
20. Pinho S, Frenette PS. Haematopoietic stem cell activity and interactions with the niche. Nat Rev Mol Cell Biol. 2019;20(5):303–20.
21. Cai H, Kondo M, Sandhow L, Xiao P, Johansson AS, Sasaki T, et al. Critical role of Lama4 for hematopoiesis regeneration and acute myeloid leukemia progression. Blood. 2022;139(20):3040–57.
22. Hoggatt J, Pelus LM. Mobilization of hematopoietic stem cells from the bone marrow niche to the blood compartment. Stem Cell Res Ther. 2011;2(2):13.
23. Tzeng YS, Li H, Kang YL, Chen WC, Cheng WC, Lai DM. Loss of Cxcl12/Sdf-1 in adult mice decreases the quiescent state of hematopoietic stem/progenitor cells and alters the pattern of hematopoietic regeneration after myelosuppression. Blood. 2011;117(2):429–39.
24. Cenariu D, Iluta S, Zimta AA, Petrushev B, Qian L, Dirzu N, et al. Extramedullary hematopoiesis of the liver and spleen. J Clin Med. 2021;10(24):5831.
25. Naveiras O, Nardi V, Wenzel PL, Hauschka PV, Fahey F, Daley GQ. Bone-marrow adipocytes as negative regulators of the haematopoietic microenvironment. Nature. 2009;460(7252):259–63.
26. Tratwal J, Rojas-Sutterlin S, Bataclan C, Blum S, Naveiras O. Bone marrow adiposity and the hematopoietic niche: a historical perspective of reciprocity, heterogeneity, and lineage commitment. Best Pract Res Clin Endocrinol Metab. 2021;35(4): 101564.
27. Zhou BO, Yu H, Yue R, Zhao Z, Rios JJ, Naveiras O, et al. Bone marrow adipocytes promote the regeneration of stem cells and haematopoiesis by secreting SCF. Nat Cell Biol. 2017;19(8):891–903.
28. Cuminetti V, Arranz L. Bone marrow adipocytes: the enigmatic components of the hematopoietic stem cell niche. J Clin Med. 2019;8(5):707.
29. Valet C, Batut A, Vauclard A, Dortignac A, Bellio M, Payrastre B, et al. Adipocyte fatty acid transfer supports megakaryocyte maturation. Cell Rep. 2020;32(1): 107875.
30. Barrachina MN, Pernes G, Becker IC, Allaeys I, Hirsch TI, Groeneveld DJ, et al. Efficient megakaryopoiesis and platelet production require phospholipid remodeling and PUFA uptake through CD36. Nat Cardiovasc Res. 2023;2(8):746–63.
31. Nies VJM, Struik D, Liu S, Liu W, Kruit JK, Downes M, et al. Autocrine FGF1 signaling promotes glucose uptake in adipocytes. Proc Natl Acad Sci USA. 2022;119(40): e2122382119.
32. Wabitsch M, Hauner H, Heinze E, Teller WM. The role of growth hormone/insulin-like growth factors in adipocyte differentiation. Metabolism. 1995;44(10 Suppl 4):45–9.
33. da Silva C, Durandt C, Kallmeyer K, Ambele MA, Pepper MS. The role of Pref-1 during adipogenic differentiation: an overview of suggested mechanisms. Int J Mol Sci. 2020;21(11):4104.
34. Jiang S, Levine JD, Fu Y, Deng B, London R, Groopman JE, et al. Cytokine production by primary bone marrow megakaryocytes. Blood. 1994;84(12):4151–6.
35. Wang J, Zhu Q, Cao D, Peng Q, Zhang X, Li C, et al. Bone marrow-derived IGF-1 orchestrates maintenance and regeneration of the adult skeleton. Proc Natl Acad Sci USA. 2023;120(1): e2203779120.
36. Xiao P, Dolinska M, Sandhow L, Kondo M, Johansson AS, Bouderlique T, et al. Sipa1 deficiency-induced bone marrow niche alterations lead to the initiation of myeloproliferative neoplasm. Blood Adv. 2018;2(5):534–48.
37. Langford DJ, Bailey AL, Chanda ML, Clarke SE, Drummond TE, Echols S, et al. Coding of facial expressions of pain in the laboratory mouse. Nat Methods. 2010;7(6):447–9.
38. Amend SR, Valkenburg KC, Pienta KJ. Murine hind limb long bone dissection and bone marrow isolation. J Vis Exp. 2016;110:53936.
39. Heib T, Gross C, Muller ML, Stegner D, Pleines I. Isolation of murine bone marrow by centrifugation or flushing for the analysis of hematopoietic cells - a comparative study. Platelets. 2021;32(5):601–7.

40. Challen GA, Boles N, Lin KK, Goodell MA. Mouse hematopoietic stem cell identification and analysis. Cytometry A. 2009;75(1):14–24.
41. Chang Y, Bluteau D, Debili N, Vainchenker W. From hematopoietic stem cells to platelets. J Thromb Haemost. 2007;5(Suppl 1):318–27.
42. Guagnano V, Furet P, Spanka C, Bordas V, Le Douget M, Stamm C, et al. Discovery of 3-(2,6-dichloro-3,5-dimethoxy-phenyl)-1-6-[4-(4-ethyl-piperazin-1-yl)-phenylamino]-pyrimidin-4-yl-1-methyl-urea (NVP-BGJ398), a potent and selective inhibitor of the fibroblast growth factor receptor family of receptor tyrosine kinase. J Med Chem. 2011;54(20):7066–83.
43. Adomshick V, Pu Y, Veiga-Lopez A. Automated lipid droplet quantification system for phenotypic analysis of adipocytes using cell profiler. Toxicol Mech Methods. 2020;30(5):378–87.
44. Livak KJ, Schmittgen TD. Analysis of relative gene expression data using real-time quantitative PCR and the 2(-Delta Delta C(T)) method. Methods. 2001;25(4):402–8.
45. Malara A, Currao M, Gruppi C, Celesti G, Viarengo G, Buracchi C, et al. Megakaryocytes contribute to the bone marrow-matrix environment by expressing fibronectin, type IV collagen, and laminin. Stem Cells. 2014;32(4):926–37.
46. Lin W, Song H, Shen J, Wang J, Yang Y, Yang Y, et al. Functional role of skeletal muscle-derived interleukin-6 and its effects on lipid metabolism. Front Physiol. 2023;14:1110926.
47. Yamamoto Y, Yamamoto H. RAGE-mediated inflammation, Type 2 diabetes, and diabetic vascular complication. Front Endocrinol. 2013;4:105.
48. He W, Wang H, Yang G, Zhu L, Liu X. The role of chemokines in obesity and exercise-induced weight loss. Biomolecules. 2024;14(9):1121.
49. Kim H, Lee MK, Kim HR. Difference in megakaryocyte expression of GATA-1, IL-6, and IL-8 associated with maintenance of platelet counts in patients with plasma cell neoplasm with dysmegakaryopoiesis. Exp Hematol. 2019;73(13–7): e2.
50. Ambele MA, Dhanraj P, Giles R, Pepper MS. Adipogenesis: a complex interplay of multiple molecular determinants and pathways. Int J Mol Sci. 2020;21(12):4283.
51. Hudak CS, Sul HS. Pref-1, a gatekeeper of adipogenesis. Front Endocrinol (Lausanne). 2013;4:79.
52. Wang Y, Sul HS. Ectodomain shedding of preadipocyte factor 1 (Pref-1) by tumor necrosis factor alpha converting enzyme (TACE) and inhibition of adipocyte differentiation. Mol Cell Biol. 2006;26(14):5421–35.
53. Challen GA, Boles NC, Chambers SM, Goodell MA. Distinct hematopoietic stem cell subtypes are differentially regulated by TGF-beta1. Cell Stem Cell. 2010;6(3):265–78.
54. Bruns I, Lucas D, Pinho S, Ahmed J, Lambert MP, Kunisaki Y, et al. Megakaryocytes regulate hematopoietic stem cell quiescence through CXCL4 secretion. Nat Med. 2014;20(11):1315–20.
55. Mendt M, Cardier JE. Role of SDF-1 (CXCL12) in regulating hematopoietic stem and progenitor cells traffic into the liver during extramedullary hematopoiesis induced by G-CSF, AMD3100 and PHZ. Cytokine. 2015;76(2):214–21.
56. Maslak P, Nimer SD. The efficacy of IL-3, SCF, IL-6, and IL-11 in treating thrombocytopenia. Semin Hematol. 1998;35(3):253–60.
57. Stork PJ, Dillon TJ. Multiple roles of Rap1 in hematopoietic cells: complementary versus antagonistic functions. Blood. 2005;106:2952–61.
58. Cardier JE, Murphy MJ Jr, Erickson-Miller CL. IL-6 interferes with stimulation of HPP-CFC and large CFU-Mk in conjunction with cytokine combinations from primitive murine marrow cells. Stem Cells. 1997;15(6):437–42.
59. Li X, Slayton WB. Molecular mechanisms of platelet and stem cell rebound after 5-fluorouracil treatment. Exp Hematol. 2013;41(7):635–45.
60. Mirantes C, Passegue E, Pietras EM. Pro-inflammatory cytokines: emerging players regulating HSC function in normal and diseased hematopoiesis. Exp Cell Res. 2014;329(2):248–54.
61. Katagiri K, Hattori M, Minato N, Kinashi T. Rap1 functions as a key regulator of T-cell and antigen-presenting cell interactions and modulates T-cell responses. Mol Cell Biol. 2002;22:1001–15.
62. Ishihara S, Nishikimi A, Umemoto E, Miyasaka M, Saegusa M, Katagiri K. Dual functions of Rap1 are crucial for T-cell homeostasis and prevention of spontaneous colitis. Nat Commun. 2015;6:1–16.
63. Zhang H, Noohr J, Jensen CH, Petersen RK, Bachmann E, Teisner B, et al. Insulin-like growth factor-1/insulin bypasses Pref-1/FA1-mediated inhibition of adipocyte differentiation. J Biol Chem. 2003;278(23):20906–14.
64. Hong KW, Jin HS, Lim JE, Ryu HJ, Go MJ, Lee JY, et al. RAPGEF1 gene variants associated with type 2 diabetes in the Korean population. Diabetes Res Clin Pract. 2009;84(2):117–22.
65. Qu L, He B, Pan Y, Xu Y, Zhu C, Tang Z, et al. Association between polymorphisms in RAPGEF1, TP53, NRF1 and type 2 diabetes in Chinese Han population. Diabetes Res Clin Pract. 2011;91(2):171–6.
66. Kanter R, Caballero B. Global gender disparities in obesity: a review. Adv Nutr. 2012;3(4):491–8.
67. Cracco RC, Bussiman FO, Polizel GHG, Furlan E, Garcia NP, Poit DAS, et al. Effects of maternal nutrition on female offspring weight gain and sexual development. Front Genet. 2021;12: 737382.
68. Samuelsson J, Alonso S, Ruiz-Larroya T, Cheung TH, Wong YF, Perucho M. Frequent somatic demethylation of RAPGEF1/C3G intronic sequences in gastrointestinal and gynecological cancer. Int J Oncol. 2011;38:1575–7.

Publisher's Note